One-dimensional kinetic description of nonlinear traveling-pulse and traveling-wave disturbances in long coasting charged particle beams

Ronald C. Davidson[1] and Hong Qin[1,2]

[1]Plasma Physics Laboratory, Princeton University, Princeton, New Jersey 08543, USA
[2]School of Nuclear Science and Technology and Department of Modern Physics, University of Science and Technology of China, Hefei, Anhui 230026, China

(Received 15 April 2015; published 21 September 2015)

This paper makes use of a one-dimensional kinetic model to investigate the nonlinear longitudinal dynamics of a long coasting beam propagating through a perfectly conducting circular pipe with radius r_w. The average axial electric field is expressed as $\langle E_z\rangle = -(\partial/\partial z)\langle\phi\rangle = -e_b g_0 \partial\lambda_b/\partial z - e_b g_2 r_w^2 \partial^3\lambda_b/\partial z^3$, where g_0 and g_2 are constant geometric factors, $\lambda_b(z,t) = \int dp_z F_b(z,p_z,t)$ is the line density of beam particles, and $F_b(z,p_z,t)$ satisfies the 1D Vlasov equation. Detailed nonlinear properties of traveling-wave and traveling-pulse (soliton) solutions with time-stationary waveform are examined for a wide range of system parameters extending from moderate-amplitudes to large-amplitude modulations of the beam charge density. Two classes of solutions for the beam distribution function are considered, corresponding to: (i) the nonlinear waterbag distribution, where $F_b = \text{const}$ in a bounded region of p_z-space; and (ii) nonlinear Bernstein-Green-Kruskal (BGK)-like solutions, allowing for both trapped and untrapped particle distributions to interact with the self-generated electric field $\langle E_z\rangle$.

DOI: 10.1103/PhysRevSTAB.18.094201 PACS numbers: 29.27.Bd, 52.25.Dg

I. INTRODUCTION

High-energy accelerators and transport systems [1–6] have a wide variety of applications ranging from basic research in high energy and nuclear physics, to applications such as spallation neutron sources, medical physics, and heavy ion fusion. As a consequence, it is increasingly important to develop an improved understanding of collective processes and the nonlinear dynamics of intense charged particle beam systems. While there has been considerable progress in three-dimensional numerical and analytical investigations of the nonlinear Vlasov-Maxwell equations describing intense beam propagation, there is also considerable interest in the development and application of simplified one-dimensional kinetic models to describe the longitudinal nonlinear dynamics of long coasting beams [7–15] in linear (linac) or large-major-radius ring geometries. The present paper employs the one-dimensional kinetic formalism recently developed by Davidson and Startsev [14] for a long coasting beam propagating through a perfecting conducting circular pipe with radius r_w. In Ref. [14] the average longitudinal electric field is expressed as $\langle E_z\rangle(z,t) = -(\partial/\partial z)\langle\phi\rangle(z,t) = -e_b g_0 \partial\lambda_b/\partial z - e_b g_2 r_w^2 \partial^3\lambda_b/\partial z^3$, where e_b is the particle charge, g_0 and g_2 are constant geometric factors that depend on the location of the conducting wall and the shape of the transverse density profile, and $\lambda_b(z,t) = \int dp_z F_b(z,p_z,t)$ is the line density. In a previous application of the 1D kinetic formalism developed in Ref. [14], the analyses in Ref. [15] assumed that the longitudinal distribution $F_b(z,p_z,t)$ corresponded to a so-called waterbag distribution [16–19], where $F_b = \text{const}$ within moving boundaries in the phase space (z,p_z). The weakly nonlinear analysis in Ref. [15] showed that disturbances moving near the sound speed evolve according to the Korteweg-deVries (KdV) equation [20–24]. The classical KdV equation, which arises in several areas of nonlinear physics in which there are cubic dispersive corrections to sound-wave-like signal propagation, also has the appealing feature that it is exactly solvable using inverse scattering techniques.

While the analysis in Ref. [15] reveals many interesting properties of the nonlinear evolution of longitudinal disturbances in intense charged particle beams, it is restricted to the weakly nonlinear regime. In the present analysis, we remove the restriction to the weakly nonlinear regime, and make use of the 1D kinetic model developed in Ref. [14], allowing for moderate to large-amplitude modulation in the charge density of the beam particles. The organization of this paper is the following. In Sec. II, the 1D kinetic model [14] is briefly reviewed (Sec. II A), and exact (local and nonlocal) nonlinear conservation constraints are derived (Sec. II B) for the conservation of particle number, momentum, and energy per unit length of the beam, making use of the nonlinear Vlasov equation for $F_b(z,p_z,t)$ in Eq. (1), and the expression for $\langle E\rangle(z,t)$ in Eq. (2). Removing the assumption of weak nonlinearity made in Ref. [15], Sec. III focuses on use of the fully nonlinear kinetic waterbag

model (Sec. III A) to investigate detailed properties of nonlinear pulselike (soliton) or periodic traveling-wave disturbances propagating with constant normalized velocity $M = \text{const}$ relative to the beam frame (Sec. III B). In normalized variables, $Z' = Z - MT$ and $T' = T$, the waveform of the disturbance is assumed to be time-stationary ($\partial/\partial T' = 0$) in the frame moving with velocity $M = \text{const}$ relative to the beam frame. Nonlinear solutions are examined over a wide range of system parameters, including regimes where the modulation in beam line density λ_b exceeds 50%, corresponding to a strongly bunched beam. Finally, in Sec. IV we examine the kinetic model based on Eqs. (9) and (10) [equivalent to Eqs. (1) and (2)] for an even broader class of distribution functions $F_b(z, p_z, t)$, recognizing that Eqs. (9) and (10) are Galilean invariant. [Keep in mind that the variables (z, p_z, t) are in the beam frame, where the particle motion is assumed to be nonrelativistic.] Introducing the appropriately scaled variables (see Sec. IV) $Z' = Z - MT$, $V_z' = V_z - M$, $T' = T$, where $M = \text{const}$, we transform Eqs. (9) and (10) to primed variables, and look for solutions that are time stationary ($\partial/\partial T' = 0$) in the frame moving with velocity $M = \text{const}$ relative to the beam frame. The analysis in Sec. IV parallels the original Bernstein-Greene-Kruskal (BGK) formulation of BGK solutions to the 1D Vlasov-Poisson equations [25,26], except for the fact that Eq. (10), which connects the effective potential $\langle\phi\rangle(z,t)$ to the line density $\lambda_b(z,t)$, has a very different structure than the 1D Poisson's equation used in the original BGK analysis. Depending on the choices of trapped-particle and untrapped-particle distribution functions, the kinetic model described in Sec. IV supports a broad range of nonlinear pulselike (soliton) solutions and periodic traveling-wave solutions that have time-stationary waveform in the frame moving with velocity $M = \text{const}$ relative to the beam frame. Similar to Sec. III B, the modulation of beam line density can have large amplitude, corresponding to a strong bunching of the beam particles. Specific examples are presented in Sec. IV corresponding to nonlinear periodic traveling-wave solutions.

II. THEORETICAL MODEL AND ASSUMPTIONS

This section provides a brief summary of the one-dimensional kinetic g-factor model (Sec. II A) developed by Davidson and Startsev [14] to describe the nonlinear longitudinal dynamics of a long coasting beam propagating in the z-direction through a circular, perfectly conducting pipe with radius r_w. The 1D kinetic Vlasov equation for the distribution function $F_b(z, p_z, t)$ is used (Sec. II B) to derive several important conservation laws (both local and global) corresponding to conservation of particle number, momentum, and energy per unit length of the charge bunch. The results in Secs. II A and II B form the basis for the nonlinear traveling-wave and traveling-pulse solutions studied in Secs. III and IV.

A. Theoretical model and assumptions

This paper makes use of a one-dimensional kinetic model [14] that describes the nonlinear dynamics of the longitudinal distribution function $F_b(z, p_z, t)$, the average self-generated axial electric field $\langle E_z\rangle(z,t)$, and the line density $\lambda_b(z,t) = \int dp_z F_b(z, p_z, t)$, for an intense charged particle beam propagating in the z-direction through a circular, perfectly conducting pipe with radius r_w. For simplicity, the analysis is carried out in the beam frame, where the longitudinal particle motion in (z, p_z) phase space is assumed to be nonrelativistic, and the beam intensity is assumed to be sufficiently low that the beam edge radius r_b and rms radius $R_b = \langle r^2\rangle^{1/2} = \langle x^2 + y^2\rangle^{1/2}$ have a negligibly small dependence on line density λ_b. Furthermore, properties such as the number density $n_b(r, z, t)$ of beam particles are assumed to be azimuthally symmetric about the beam axis ($\partial/\partial\theta = 0$), where $x = r\cos\theta$ and $y = r\sin\theta$ are cylindrical polar coordinates. Finally, the axial spatial variation in the line density $\lambda_b(z,t) = 2\pi\int_0^{r_w} drrn_b(r,z,t)$ is assumed to be sufficiently slow that $k_z^2 r_w^2 \ll 1$, where $\partial/\partial z \backsim k_z \backsim L_z^{-1}$ is the inverse length scale of the z-variation of beam properties.

Making use of these assumptions, it can be shown that the one-dimensional kinetic equation describing the nonlinear evolution of the longitudinal distribution function $F_b(z, p_z, t)$ and average longitudinal electric field $\langle E_z\rangle(z,t)$ can be expressed in the beam frame correct to order $k_z^2 r_w^2$ as [14]

$$\frac{\partial}{\partial t}F_b + v_z\frac{\partial}{\partial z}F_b + e_b\langle E_z\rangle\frac{\partial}{\partial p_z}F_b = 0, \tag{1}$$

and

$$\frac{e_b}{m_b}\langle E_z\rangle = -\frac{U_{b0}^2}{\lambda_{b0}}\frac{\partial}{\partial z}\lambda_b - \frac{r_w^2 U_{b2}^2}{\lambda_{b0}}\frac{\partial^3\lambda_b}{\partial z^3}. \tag{2}$$

Here, e_b and m_b are the charge and rest mass of a beam particle, and $\lambda_{b0} = \text{const}$ is a measure of the characteristic line density of beam particles, e.g., its average value. Moreover, the constants U_{b0}^2 and U_{b2}^2 have dimensions of speed-squared, and are defined by

$$U_{b0}^2 = \frac{\lambda_{b0}g_0 e_b^2}{m_b}, \qquad U_{b2}^2 = \frac{\lambda_{b0}g_2 e_b^2}{m_b}, \tag{3}$$

where g_0 and g_2 are the geometric factors defined by [14]

$$g_0 = 2\int_0^{r_w}\frac{dr}{r}\left(2\pi\int_0^r drr\frac{n_b}{\lambda_b}\right)^2, \tag{4}$$

$$g_2 = \frac{2}{r_w^2}\int_0^{r_w}\frac{dr}{r}2\pi\left(\int_0^r drr\frac{n_b}{\lambda_b}\right) \times\int_0^r drr\int_r^{r_w}\frac{dr}{r}\left(2\pi\int_0^r drr\frac{n_b}{\lambda_b}\right). \tag{5}$$

In obtaining Eqs. (1)–(5), a perfectly conducting cylindrical wall with $E_z(r = r_w, z, t) = 0$ has been assumed.

For the purposes of illustration, we consider the class of axisymmetric density profiles $n_b(r, z, t)$ of the form

$$n_b = \begin{cases} \frac{\lambda_b}{\pi r_b^2} f(\frac{r}{r_b}), & 0 \le r < r_b, \\ 0, & r_b < r \le r_w. \end{cases} \tag{6}$$

Here, $\lambda_b = \int dp_z F_b(z, p_z, t) = 2\pi \int_0^{r_w} drrn_b(r, z, t)$ is the line density, r_b is the beam edge radius, assumed independent of λ_b, and $f(r/r_b)$ is the profile shape function with normalization $\int_0^1 dxxf(x) = 1/2$. As an example, for $f(r/r_b) = (n+1)(1 - r^2/r_b^2)^n$, $n = 0, 1, 2, \ldots$, over the interval $0 \le r < r_b$, it can be shown that [14]

$$g_0 = \ln\left(\frac{r_w^2}{r_b^2}\right) + \sum_{m=1}^{n+1} \frac{n+1}{m(m+n+1)}, \tag{7}$$

$$g_2 = \frac{1}{2}\left[1 - \frac{1}{(n+2)}\frac{r_b^2}{r_w^2}\left(1 + \ln\frac{r_w^2}{r_{b^2}}\right) - \sum_{m=1}^{n+1} \frac{1}{m(m+n+2)}\frac{r_b^2}{r_w^2}\right]. \tag{8}$$

From Eqs. (6)–(8), we note that $n = 0$ corresponds to a step-function density profile; $n = 1$ corresponds to a parabolic density profile; $n \ge 2$ corresponds to an even more peaked density profile; and that the precise values of g_0 and g_2 depend on the profile shape [14]. Finally, for the choice of shape function $f(r/r_b) = (n+1)(1 - r^2/r_b^2)^n$, $n = 0, 1, 2, \ldots$, it is readily shown that the mean-square beam radius is $R_b^2 = \lambda_b^{-1} 2\pi \int_0^{r_w} drrr^2 n_b = (n+2)^{-1} r_b^2$, so that for fixed value of rms radius R_b, the edge radius r_b increases with increasing value of the density profile shape factor n.

B. Conservation relations

Equations (1) and (2) possess several important conservation laws, both local and global, corresponding to conservation of particle number, momentum, and energy per unit length. For present purposes we express $\langle E_z\rangle(z,t) = -(\partial/\partial z)\langle\phi\rangle(z,t)$. Equations (1) and (2) then describe the evolution of $F_b(z, p_z, t)$ and $\langle\phi\rangle(z,t)$ according to

$$\frac{\partial}{\partial t}F_b + v_z\frac{\partial}{\partial z}F_b - e_b\frac{\partial\langle\phi\rangle}{\partial z}\frac{\partial F_b}{\partial p_z} = 0, \tag{9}$$

where $v_z = p_z/m_b$ and

$$e_b\frac{\partial}{\partial z}\langle\phi\rangle = m_b U_{b0}^2\frac{\partial}{\partial z}N_b + m_b U_{b2}^2 r_w^2\frac{\partial^3}{\partial z^3}N_b. \tag{10}$$

Here,

$$N_b(z,t) = \frac{\lambda_b(z,t)}{\lambda_{b0}} = \lambda_{b0}^{-1}\int dp_z F_b(z, p_z, t) \tag{11}$$

is a dimensionless measure of the line density $\lambda_b(z,t)$, and $\lambda_{b0} = \text{const}$ is the characteristic (e.g., average) value of line density.

It is convenient to introduce the macroscopic moments

$$N_b V_b = N_b\langle v_z\rangle = \lambda_{b0}^{-1}\int dp_z v_z F_b, \tag{12}$$

$$N_b\langle v_z^n\rangle = \lambda_{b0}^{-1}\int dp_z v_z^n F_b, \tag{13}$$

where $N_b = \lambda_b/\lambda_{b0}$ is defined in Eq. (11), and $V_b(z,t) = (\int dp_z v_z F_b)/(\int dp_z F_b)$ is the average axial flow velocity in the beam frame. Note that the effective "pressure" $P_b(z,t)$ and "heat flow" $Q_b(z,t)$ are defined (relative to the average flow velocity V_b) by

$$P_b(z,t) = \lambda_{b0}N_b m_b\langle(v_z - V_b)^2\rangle = m_b\int dp_z(v_z - V_b)^2 F_b, \tag{14}$$

and

$$Q_b(z,t) = \lambda_{b0}N_b m_b\langle(v_z - V_b)^3\rangle = m_b\int dp_z(v_z - V_b)^3 F_b, \tag{15}$$

where $V_b(z,t)$ is the average flow velocity defined in Eq. (12).

We now make use of Eqs. (9) and (10) to derive the *local* and *global* conservation laws corresponding to the conservation of particle number, momentum, and energy per unit length of the beam. The subsequent analysis applies to the two classes of beam systems: (i) a very long, finite-length charge bunch ($L_b \gg r_w$) with $N_b(z \to \pm\infty, t) = 0$; and (ii) a circulating beam in a large-aspect-ratio ($R_0 \gg r_w$) ring with periodic boundary condition $N_b(z + 2\pi R_0, t) = N_b(z,t)$ as the beam circulates around the ring with major radius R_0. (Here, z can be viewed as the arc length around the perimeter of the ring with large radius R_0.)

1. Number conservation

From Eqs. (9), (11), and (12), operating on Eq. (9) with $\lambda_{b0}^{-1}\int dp_z \cdots$, and integrating by parts with respect to p_z, we obtain

$$\frac{\partial}{\partial t}N_b + \frac{\partial}{\partial z}(N_b V_b) = 0, \tag{16}$$

where $N_b(z,t) = \lambda_b(z,t)/\lambda_{b0}$ is the normalized line density, and $V_b(z,t)$ is the axial flow velocity [Eqs. (11) and (12)]. Equation (16) is a statement of local number conservation, i.e., the time rate of change of the local density, $\partial N_b/\partial t$, is equal to minus the derivative of the local flux of particles, $-(\partial/\partial z)(N_b V_b)$. If we integrate

Eq. (16) over z, applying the boundary conditions described earlier in this section, we obtain

$$\frac{\partial}{\partial t}\int dz N_b = 0, \tag{17}$$

which corresponds to the *global* conservation of the number of beam particles.

2. Momentum conservation

We now operate on Eq. (9) with $\lambda_{b0}^{-1}\int dp_z p_z \cdots$, where $p_z = m_b v_z$, and make use of Eqs. (12) and (13). This gives

$$\frac{\partial}{\partial t}N_b m_b V_b + \frac{\partial}{\partial z}N_b m_b \langle v_z v_z\rangle + e_b N_b \frac{\partial}{\partial z}\langle\phi\rangle = 0, \tag{18}$$

where $-(\partial/\partial z)\langle\phi\rangle$ is defined in Eq. (10), and we have integrated by parts with respect to p_z to obtain Eq. (18) from Eq. (9). Equation (18) can be expressed in an alternate form by making use of Eq. (10) to eliminate $e_b(\partial/\partial z)\langle\phi\rangle$ and combine Eqs. (12)–(14) to express

$$N_b m_b\langle v_z v_z\rangle = N_b m_b V_b V_b + \lambda_{b0}^{-1}P_b, \tag{19}$$

where $V_b(z,t)$ is the average flow velocity, and $P_b(z,t)$ is the effective pressure of the beam particles. Substituting Eqs. (10) and (19) into Eq. (18), we obtain

$$\begin{aligned}&\frac{\partial}{\partial t}N_b m_b V_b + \frac{\partial}{\partial z}\{N_b m_b V_b V_b + \lambda_{b0}^{-1}P_b\}\\ &\quad + N_b m_b\left\{U_{b0}^2\frac{\partial N_b}{\partial z} + U_{b2}^2 r_w^2\frac{\partial^3 N_b}{\partial z^3}\right\}\\ &= \frac{\partial}{\partial t}N_b m_b V_b + \frac{\partial}{\partial z}\left\{N m_b V_b V_b + \lambda_{b0}^{-1}P_b + \frac{1}{2}m_b U_{b0}^2 N_b^2\right\}\\ &\quad + \frac{\partial}{\partial z}\left\{m_b U_{b2}^2 r_w^2\left[N_b\frac{\partial^2 N_b}{\partial z^2} - \frac{1}{2}\left(\frac{\partial N_b}{\partial z}\right)^2\right]\right\} = 0.\end{aligned} \tag{20}$$

Note that Eq. (20) expresses the *local* force balance equation in the form of a *local* conservation relation for the momentum density of a beam fluid element. Moreover, integrating Eq. (20) over z and applying the boundary conditions described earlier in Sec. II gives

$$\frac{\partial}{\partial t}\int dz N_b m_b V_b = 0, \tag{21}$$

which corresponds to *global* momentum conservation.

3. Energy conservation

We now operate on Eq. (9) with $\lambda_{b0}^{-1}\int dp_z \frac{1}{2}m_b v_z^2 \cdots$ and make use of Eqs. (11)–(13) and $p_z = m_b v_z$. Integrating by parts with respect to p_z, we readily obtain

$$\begin{aligned}&\frac{\partial}{\partial z}\left(\frac{1}{2}N_b m_b\langle v_z^2\rangle\right) + \frac{\partial}{\partial z}\left(\frac{1}{2}N_b m_b\langle v_z^3\rangle\right) + e_b\frac{\partial\langle\phi\rangle}{\partial z}N_b V_b\\ &\quad = 0.\end{aligned} \tag{22}$$

From Eqs. (10) and (16), some straightforward algebraic manipulation gives

$$\begin{aligned}e_b\frac{\partial\langle\phi\rangle}{\partial z}N_b V_b &= \frac{\partial}{\partial z}\left[\frac{1}{2}m_b U_{b0}^2 N_b^2 - \frac{1}{2}m_b U_{b2}^2 r_w^2\left(\frac{\partial N_b}{\partial z}\right)^2\right]\\ &\quad + \frac{\partial}{\partial z}\left\{m_b U_{b0}^2(N_b N_b V_b) + m_b U_{b2}^2 r_w^2\right.\\ &\quad \left.\times\left[N_b V_b\frac{\partial^2 N_b}{\partial z^2} + \frac{\partial N_b}{\partial z}\frac{\partial N_b}{\partial t}\right]\right\}.\end{aligned} \tag{23}$$

Substituting Eq. (23) into Eq. (22) and rearranging terms, we obtain

$$\begin{aligned}&\frac{\partial}{\partial t}\left\{\frac{1}{2}N_b m_b\langle v_z^2\rangle + \frac{1}{2}m_b U_{b0}^2 N_b^2 - \frac{1}{2}m_b U_{b2}^2 r_w^2\left(\frac{\partial N_b}{\partial z}\right)^2\right\}\\ &\quad + \frac{\partial}{\partial z}\left\{\frac{1}{2}N_b m_b\langle v_z^3\rangle + m_b U_{b0}^2 N_b^2 V_b + m_b U_{b2}^2 r_w^2\right.\\ &\quad \left.\times\left[N_b V_b\frac{\partial^2 N_b}{\partial z^2} + \frac{\partial N_b}{\partial z}\frac{\partial N_b}{\partial t}\right]\right\} = 0,\end{aligned} \tag{24}$$

which corresponds to *local* conservation of energy. *Global* energy conservation follows upon integrating Eq. (24) over z, which gives

$$\begin{aligned}&\frac{\partial}{\partial t}\int dz\left\{\frac{1}{2}N_b m_b\langle v_z^2\rangle + \frac{1}{2}m_b U_{b0}^2 N_b^2 - \frac{1}{2}m_b U_{b2}^2 r_w^2\left(\frac{\partial N_b}{\partial z}\right)^2\right\}\\ &\quad = 0.\end{aligned} \tag{25}$$

Note that Eq. (25) describes the balance in energy exchange between particle kinetic energy and electrostatic field energy. Moreover, the final two terms inside curly brackets in Eq. (25) correspond to electrostatic field energy, and the term inside the curly brackets proportional to U_{b0}^2 is positive, whereas the term proportional to U_{b2}^2 is manifestly negative. Because of the negative sign of the third term in Eq. (25), note that any increase in $(\partial N_b/\partial z)^2$ averaged over z must compensated by a corresponding increase in the first two terms in Eq. (25).

To summarize, the *local* conservation laws in Eqs. (16), (18), and (24), and the *global* conservation laws in Eqs. (17), (21), and (25), provide powerful nonlinear constrains on the evolution of the normalized line density N_b, momentum density $N_b m_b V_b$, and kinetic energy density $N_b m_b\langle v_z^2\rangle/2 = N_b m_b V_b^2/2 + \lambda_{b0}^{-1}P_b/2$. Furthermore, these conservation constraints are exact consequences of the 1D nonlinear Vlasov equation (9) for $F_b(z,p_z,t)$, where $e_b(\partial/\partial z)\langle\phi\rangle(z,t)$ is defined in Eq. (10), and U_{b0}^2 and U_{b2}^2 are expressed in terms of the geometric factors g_0 and g_2 in Eq. (3).

Finally, the energy balance equation (22), the momentum balance equation (18), and the continuity equation (16) can be combined to give a dynamical equation for the evolution of the effective pressure $P_b(z,t)$ of the beam particles. We make use of $N_b m_b \langle v_z^2 \rangle = N_b m_b V_b^2 + \lambda_{b0}^{-1} P_b$, to express

$$\begin{aligned} N_b m_b \langle v_z^3 \rangle &= N_b m_b \langle (v_z - V_b + V_b)^3 \rangle \\ &= N_b m_b V_b^3 + 3 N_b m_b V_b \langle (v_z - V_b)^2 \rangle \\ &\quad + N_b m_b \langle (v_z - V_b)^3 \rangle \\ &= N_b m_b V_b^3 + 3 N_b V_b \lambda_{b0}^{-1} P_b + \lambda_{b0}^{-1} Q_b, \end{aligned} \tag{26}$$

where Q_b is the effective heat flow defined in Eq. (15). Without presenting algebraic details, some straightforward manipulation of Eq. (22) that makes use of Eqs. (16) and (18) then gives

$$\left(\frac{\partial}{\partial t} + V_b \frac{\partial}{\partial z} \right) P_b + 3 P_b \frac{\partial V_b}{\partial z} + \frac{\partial}{\partial z} Q_b = 0. \tag{27}$$

To summarize, Eqs. (16), (20), and (27) describe the self-consistent nonlinear evolution of $N_b(z,t)$, $V_b(z,t)$ and $P_b(z,t)$. In the special case where the heat flow contribution $(\partial/\partial z) Q_b$ is *negligibly small* in Eq. (27), the pressure $P_b(z,t)$ evolves *approximately* according to

$$\left(\frac{\partial}{\partial t} + V_b \frac{\partial}{\partial z} \right) P_b + 3 P_b \frac{\partial V_b}{\partial z} = 0. \tag{28}$$

The continuity equation (16) can be expressed as

$$\left(\frac{\partial}{\partial t} + V_b \frac{\partial}{\partial z} \right) N_b + N_b \frac{\partial V_b}{\partial z} = 0. \tag{29}$$

Combining Eqs. (27) and (28), we obtain

$$\left(\frac{\partial}{\partial t} + V_b \frac{\partial}{\partial z} \right) \left(\frac{P_b}{N_b^3} \right) = 0, \tag{30}$$

which can be integrated to give the triple-adiabatic pressure relation $(P_b/N_b^3) = \text{const}$. Therefore, for negligibly small heat flow in Eq. (27), the macroscopic fluid model obtained by taking moments of the 1D Vlasov equation (9) closes, and the nonlinear evolution of N_b, V_b and P_b is described by Eqs. (16), (20), and (30).

In Sec. III, we discuss a particular choice of distribution function $F_b(z, p_z, t)$, corresponding to the so-called waterbag distribution, for which the heat flow $Q_b(z,t)$ is exactly zero during the nonlinear evolution of the system. In this case, the closure is exact, and the nonlinear evolution of the system is fully described by Eqs. (16), (20), and (30).

III. COHERENT NONLINEAR STRUCTURES OBTAINED FROM THE KINETIC WATERBAG MODEL

The 1D kinetic g-factor model based on Eqs. (1) and (2) can be used to determine the nonlinear evolution of the beam distribution function $F_b(z, p_z, t)$ for a broad range of system parameters and initial distribution functions. In this section, we examine Eqs. (1) and (2) for the class of exact solutions for $F_b(z, p_z, t)$ corresponding to the so-called waterbag distribution in which $F_b(z, p_z, t)$ has uniform density in phase space (Sec. III A). The subclass of coherent nonlinear traveling-wave and traveling-pulse solutions with undistorted waveform are then examined (Sec. III B) for disturbances traveling in the longitudinal direction with constant normalized velocity $M = \text{const}$.

A. Kinetic Waterbag model

Equations (1) and (2), or equivalently, Eqs. (9) and (10) constitute the starting point in the present 1D kinetic description of the longitudinal nonlinear dynamics of a long coasting beam. The detailed wave excitations associated with Eqs. (9) and (10) of course depend on the form of the distribution function $F_b(z, p_z, t)$. For small-amplitude perturbations, Eqs. (1) and (2) support solutions corresponding to sound-wave-like disturbances with signal speed depending on U_{b0} and the momentum spread of F_b, and cubic dispersive modifications depending on U_{b2} [14].

In this section, we specialize to the class of exact nonlinear solutions for $F_b(z, p_z, t)$ to Eq. (1) corresponding to the waterbag distribution [15–19]

$$F_b(z, p_z, t) = \begin{cases} A = \text{const}, & m V_b^-(z,t) < p_z < m_b V_b^+(z,t), \\ 0, & \text{otherwise}, \end{cases} \tag{31}$$

for $-\infty < z < \infty$ (long coasting beam in linear geometry) or $0 < z < 2\pi R_0$ (large-aspect-ratio ring with major radius R_0). In Eq. (31), the distribution function $F_b = A$ remains constant within the boundary curves $m_b V_b^-$ and $m_b V_b^+$, and zero outside. The boundary curves, $m_b V_b^-(z,t)$ and $m_b V_b^+(z,t)$, are assumed to be single-valued, and of course the boundary curves distort nonlinearly as the system evolves according to Eqs. (1) and (2) [or equivalently, Eqs. (9) and (10)]. We integrate across the two boundary curves in Eq. (31) by operating on Eq. (1) with

$$\begin{aligned} &\lim_{\epsilon \to 0^+} \int_{m_b V_b^-(1-\epsilon)}^{m_b V_b^-(1+\epsilon)} dp_z p_z \cdots, \quad \text{and} \\ &\lim_{\epsilon \to 0^+} \int_{m_b V_b^+(1-\epsilon)}^{m_b V_b^+(1+\epsilon)} dp_z p_z \cdots, \end{aligned} \tag{32}$$

where $p_z = m_b v_z$. Integrating by parts with respect to p_z, and taking the limit $\epsilon \to 0^+$, we obtain for the nonlinear evolution of the boundary curves $V_b^-(z,t)$ and $V_b^+(z,t)$

$$\frac{\partial}{\partial t}V_b^- + V_b^-\frac{\partial}{\partial z}V_b^- = \frac{e_b}{m_b}\langle E_z\rangle, \tag{33}$$

$$\frac{\partial}{\partial t}V_b^+ + V_b^+\frac{\partial}{\partial z}V_b^+ = \frac{e_b}{m_b}\langle E_z\rangle, \tag{34}$$

where $\langle E_z\rangle$ is defined in Eq. (2).

To summarize, for each value of z, the waterbag distribution in Eq. (31) has a flat-top distribution in p_z (also called a "top-hat" distribution) between the boundary curves $p_z = m_b V_b^-(z,t)$ and $p_z = m_b V_b^+(z,t)$. While the momentum derivative proportional to $\partial F_b/\partial p_z$ becomes singular at the boundaries, $p_z = m_b V_b^-(z,t)$ and $p_z = m_b V_b^+(z,t)$, for the choice of waterbag distribution in Eq. (31), it is precisely this delta-function singularity that permits the integration in Eq. (32) over the Vlasov equation (1) to be carried out exactly, leading to the dynamical equations (33) and (34) for the boundary curves $m_b V_b^-(z,t)$ and $m_b V_b^+(z,t)$. Indeed, for the choice of waterbag distribution in Eq. (31), the nonlinear Vlasov equation (1) is exactly equivalent to the two dynamical equations (33) and (34) for $V_b^-(z,t)$ and $V_b^+(z,t)$. Furthermore, it can be shown exactly that if $F_b(z,p_z,t)$ has the form of the waterbag distribution in Eq. (31) at $t=0$, then the flat-top waterbag form is maintained at all subsequent times t by the Vlasov equation (1), where the boundary curves $m_b V_b^-(z,t)$ and $m_b V_b^+(z,t)$ evolve nonlinearly according to Eqs. (33) and (34), and $\langle E_z\rangle$ is determined from Eq. (2).

The positive features of the choice of waterbag distribution function in Eq. (31) in simplifying the analysis of the nonlinear Vlasov-Poisson equations (1) and (2) will become apparent in the remainder of Sec. III. In this regard, it is important to recognize that beam distribution functions typically tend to be smooth, differentiable functions with respect to z and p_z, rather than have singular derivatives, as does the distribution in Eq. (31) with respect to p_z. For this reason, in Sec. IV we describe a more general formulation of nonlinear, coherent structures and traveling-wave solutions to the Vlasov-Poisson equations (1) and (2) that accommodates smooth distribution functions F_b [see Eqs. (76) and (89) in Sec. IV]. It is certainly the case that the detailed shape of the distribution function in phase space (z,p_z) can have an important influence on beam stability properties and collective excitations [1,14,15]. Nonetheless, what is also noteworthy is the fact that the waterbag model does a very good job in describing the nonlinear evolution of the beam line density, beam flow velocity, and beam particle pressure in circumstances where the heat low Q_b can be treated as negligibly small [compare Eqs. (27) and (41), and see related discussions].

For the choice of waterbag distribution in Eq. (31), we calculate several macroscopic fluid quantities [see also Eqs. (11)–(15)] corresponding to line density

$$\lambda_b = \int dp_z F_b = A m_b (V_b^+ - V_b^-), \tag{35}$$

axial flow velocity

$$V_b = \lambda_b^{-1}\int dp_z v_z F_b = \frac{1}{2}(V_b^+ + V_b^-), \tag{36}$$

beam particle pressure

$$P_b = m_b\int dp_z (v_z - V_b)^2 F_b = \frac{1}{12}m_b^2 A (V_b^+ - V_b^-)^3 = \frac{1}{12 m_b A^2}\lambda_b^3, \tag{37}$$

and beam particle heat flow

$$Q_b = m_b\int dp_z (v_z - V_b)^3 F_b = 0. \tag{38}$$

Note that the heat flow is exactly $Q_b = 0$ for the choice of waterbag distribution in Eq. (31).

Making use of the dynamical equations for $V_b^-(z,t)$ and $V_b^+(z,t)$ in Eqs. (33) and (34), where $\langle E_z\rangle$ is defined in Eq. (2), some straightforward algebra shows that $\lambda_b(z,t)$, $V_b(z,t)$, and $P_b(z,t)$ evolve according to [15]

$$\frac{\partial}{\partial t}\lambda_b + \frac{\partial}{\partial z}(\lambda_b V_b) = 0, \tag{39}$$

$$\lambda_b\left(\frac{\partial}{\partial t}V_b + V_b\frac{\partial}{\partial z}V_b\right) + \frac{1}{m}\frac{\partial P_b}{\partial z} = -\lambda_b\left(\frac{U_{b0}^2}{\lambda_{b0}}\frac{\partial}{\partial z}\lambda_b + \frac{U_{b2}^2 r_w^2}{\lambda_{b0}}\frac{\partial^3\lambda_b}{\partial z^3}\right), \tag{40}$$

$$\left(\frac{\partial}{\partial t} + V_b\frac{\partial}{\partial z}\right)\left(\frac{P_b}{\lambda_b^3}\right) = 0. \tag{41}$$

Note from Eqs. (37) and (41) that $P_b(z,t)$ can be expressed as

$$P_b(z,t) = \frac{P_{b0}}{\lambda_{b0}^3}\lambda_b^3(z,t), \tag{42}$$

where $P_{b0} = \text{const}$ and $\lambda_{b0} = \text{const}$ represent the characteristic (e.g., average) values of the pressure and line density, respectively, of the beam particles, and $P_{b0}/\lambda_{b0}^3 = 1/12 m_b A^2 = \text{const}$, where A is the constant phase-space density in Eq. (31). By virtue of the fact that the heat flow $Q_b(z,t) = 0$ exactly for the choice of distribution function $F_b(z,p_z,t)$ in Eq. (31), it is not surprising that Eqs. (39)–(42) are identical to the macroscopic fluid equations (16), (20) and (30), obtained in Sec. II B, where Eq. (30) has made the assumption of negligible heat flow in Eq. (27).

Note here that $N_b(z,t)$ and $\lambda_b(z,t)$ are related by $N_b(z,t) = \lambda_b(z,t)/\lambda_{b0}$.

For the present purposes, we introduce the effective thermal speed U_{bT} associated with the waterbag distribution in Eq. (31) defined by

$$U_{bT}^2 = \frac{3P_{b0}}{\lambda_{b0} m_b}, \tag{43}$$

and the normalized (dimensionless) fluid quantities $\eta(z,t)$ and $U(z,t)$ defined by

$$\eta = N_b - 1 = \frac{\lambda_b - \lambda_{b0}}{\lambda_{b0}}, \qquad U = \frac{V_b}{(U_{b0}^2 + U_{bT}^2)^{1/2}}. \tag{44}$$

In Eq. (44), $(U_{b0}^2 + U_{bT}^2)^{1/2}$ is the effective sound speed associated with the geometric factor g_0 and the thermal speed U_{bT}. Furthermore, we introduce the scaled (dimensionless) time variable T and spatial variable Z defined by

$$T = \left(\frac{U_{b0}^2 + U_{bT}^2}{U_{b2}^2}\right)\frac{U_{b2}t}{r_w}, \qquad Z = \left(\frac{U_{b0}^2 + U_{bT}^2}{U_{b2}^2}\right)^{1/2}\frac{z}{r_w}. \tag{45}$$

Making use of the macroscopic equations (39), (40), and (42), and the definitions in Eqs. (43)–(45), it is straightforward to show that the continuity equation (39) and force balance equation (40) reduce in dimensionless variables exactly to

$$\frac{\partial}{\partial T}\eta + \frac{\partial}{\partial Z}(U + \eta U) = 0, \tag{46}$$

$$\frac{\partial}{\partial T}U + \frac{\partial}{\partial Z}\left(\frac{1}{2}U^2 + \eta + \frac{1}{2}\frac{U_{bT}^2}{U_{b0}^2 + U_{bT}^2}\eta^2 + \frac{\partial^2}{\partial Z^2}\eta\right) = 0. \tag{47}$$

The fluid description in scaled variables provided by Eqs. (46) and (47) is exactly equivalent to the kinetic description provided by Eqs. (1) and (2) for the choice of waterbag distribution in Eq. (31).

B. Coherent nonlinear traveling-wave and traveling-pulse solutions

Within the context of the present 1D model, Eqs. (46) and (47) can be used to investigate detailed properties of collective excitations over a wide range of system parameters. For example, in the weakly nonlinear regime, for small-amplitude disturbances moving near the sound speed $(U_{b0}^2 + U_{bT}^2)^{1/2}$, Eqs. (46) and (47) can be shown to reduce to the Korteweg-deVries equation [15], which exhibits the generation and interaction of coherent structures (solitons) for a wide range of initial density perturbations $\eta(Z, T=0) \neq 0$ [22]. While the analysis in Ref. [15] has several interesting features, the results are limited to the weakly nonlinear regime where $|\eta| \ll 1$ and $|U| \ll 1$.

In this paper, we examine Eqs. (46) and (47) in circumstances where there are no *a priori* restrictions to small amplitude, i.e., $\eta = (\lambda_b - \lambda_{b0})/\lambda_{b0}$ is allowed to be of order unity, as long as $\lambda_b/\lambda_{b0} > 0$, which corresponds to $\eta > -1$. Furthermore, we look for solutions to Eqs. (46) and (47) that depend on Z and T exclusively through the variables $Z' = Z - MT$ and $T' = T$, where $M = \text{const}$ is the normalized pulse speed measured in units of the sound speed $(U_{b0}^2 + U_{bT}^2)^{1/2}$. Making use of $\partial/\partial Z = \partial/\partial Z'$ and $\partial/\partial T = \partial/\partial T' - M\partial/\partial Z'$ and looking for time-stationary solutions $(\partial/\partial T' = 0)$ in the frame of reference moving with normalized velocity $M = \text{const}$, Eqs. (46) and (47) for $\eta(Z')$ and $U(Z')$ become

$$\frac{\partial}{\partial Z'}[(-M + U)\eta + U] = 0, \tag{48}$$

$$\frac{\partial}{\partial Z'}\left[\frac{1}{2}U^2 - MU + \eta + \frac{1}{2}\frac{U_{bT}^2}{U_{b0}^2 + U_{bT}^2}\eta^2 + \frac{\partial^2\eta}{\partial Z'^2}\right] = 0. \tag{49}$$

Integrating with respect to Z', Eqs. (48) and (49) give

$$-M\eta + (1+\eta)U = \text{const}, \tag{50}$$

$$\frac{1}{2}U^2 - MU + \eta + \frac{1}{2}\frac{U_{bT}^2}{U_{b0}^2 + U_{bT}^2}\eta^2 + \frac{\partial^2\eta}{\partial Z'^2} = \text{const}, \tag{51}$$

which relate $\eta(Z')$ and $U(Z')$, where $Z' = Z - MT$.

The solutions for $\eta(Z')$ and $U(Z')$ to Eqs. (50) and (51) depend on the values of the constants in Eqs. (50) and (51). For the present purposes we consider boundary conditions such that $U = 0$ when $\eta = 0$, and $\eta'' = 0$ when $U = 0$ and $\eta = 0$. In this case the values of the constants in Eqs. (50) and (51) are zero, which gives

$$U = M\frac{\eta}{1+\eta}. \tag{52}$$

$$\frac{\partial^2\eta}{\partial Z'^2} + \left\{\frac{1}{2}(U - M)^2 - \frac{1}{2}M^2 + \eta + \frac{1}{2}\frac{U_{bT}^2}{U_{b0}^2 + U_{bT}^2}\eta^2\right\} = 0. \tag{53}$$

Substituting Eq. (52) into Eq. (53), we obtain

$$\frac{\partial^2\eta}{\partial Z'^2} + \left\{\frac{1}{2}M^2\left[\frac{1}{(1+\eta)^2} - 1\right] + \eta + \frac{1}{2}\frac{U_{bT}^2}{U_{b0}^2 + U_{bT}^2}\eta^2\right\} = 0, \tag{54}$$

which is a second-order nonlinear differential equation for the perturbation in line density $\eta(Z') = [\lambda_b(Z') - \lambda_{b0}]/\lambda_{b0}$, where $Z' = Z - MT$. Some straightforward algebraic manipulation shows that Eq. (54) can be expressed in the equivalent form

$$\frac{\partial^2\eta}{\partial Z'^2} = -\frac{\partial}{\partial\eta}V(\eta), \tag{55}$$

where $V(\eta)$ is the effective potential defined by

$$V(\eta) = \frac{1}{2}\frac{\eta^2}{1+\eta}\{\epsilon_T\eta^2 + (1+\epsilon_T)\eta + (1-M^2)\}, \tag{56}$$

and the dimensionless parameter ϵ_T, defined by

$$\epsilon_T = \frac{1}{3}\left(\frac{U_{bT}^2}{U_{b0}^2 + U_{bT}^2}\right), \tag{57}$$

is a measure of the longitudinal thermal speed of the beam particles.

Equations (55) and (56) can be used to determine the solutions for $\eta(Z')$ for a broad range of dimensionless parameters ϵ_T and M. Furthermore, Eqs. (55) and (56) have been obtained from Eqs. (50) and (51) for the special class of boundary conditions where $U = 0$ and $\eta'' = 0$ when $\eta = 0$ [see discussion prior to Eqs. (52) and (53)]. Indeed, we will show below that Eqs. (55) and (56) support two classes of solutions consistent with these boundary conditions. These correspond to: (i) localized (pulselike) soliton solutions when $M^2 > 1$, satisfying $\eta(Z' = \pm\infty) = 0$, $U(Z' = \pm\infty) = 0$, and $[\partial^2\eta/\partial Z'^2]_{Z'=\pm\infty} = 0$; and (ii) nonlinear periodic traveling-wave solutions when $M^2 < 1$, with $\eta(Z') = \eta(Z'+L)$, and $\eta(Z'=0) = 0$, $U(Z' = 0) = 0$, and $[\partial^2\eta/\partial Z'^2]_{Z'=0} = 0$.

In general, the effective potential $V(\eta)$ in Eq. (57) can be expressed as

$$V(\eta) = \frac{1}{2}\frac{\eta^2}{1+\eta}\epsilon_T[(\eta-\eta^+)(\eta-\eta^-)], \tag{58}$$

where

$$\eta^\pm = \frac{1}{2}\left\{-\left(1+\frac{1}{\epsilon_T}\right) \pm \left[\left(1+\frac{1}{\epsilon_T}\right)^2 + \frac{4}{\epsilon_T}(M^2-1)^{1/2}\right]\right\}. \tag{59}$$

In Eqs. (58) and (59), ϵ_T is restricted to the range $0 < \epsilon_T < 1/3$, and M^2 can satisfy $M^2 > 1$ or $M^2 < 1$. Examination of Eq. (59) shows that

$$\eta^- < -1, \qquad \eta^+ > -1, \tag{60}$$

for all allowed values of ϵ_T and M^2. Furthermore, it is also clear from Eq. (59) that

$$\begin{cases} \eta^+ > 0, & \text{for } M^2 > 1, \\ \eta^+ < 0, & \text{for } M^2 < 1. \end{cases} \tag{61}$$

Recall that $\eta = (\lambda_b - \lambda_{b0})/\lambda_{b0}$. Then $\lambda_b/\lambda_{b0} \geq 0$ implies that $\eta \geq -1$ is the region of interest physically for solutions to Eq. (55).

Note that Eq. (55) has the form of a dynamical equation of motion, with η playing the role of displacement, Z' playing the role of time, and $V(\eta)$ playing the role of an effective potential, or so-called pseudopotential. Multiplying Eq. (55) by $\partial\eta/\partial Z'$ and integrating, we obtain

$$\frac{1}{2}\left(\frac{\partial\eta}{\partial Z'}\right)^2 + V(\eta) = E = \text{const} \tag{62}$$

Equation (62) plays the role of an effective energy conservation constraint, and can be integrated to determine $\eta(Z')$ for the pseudopotential $V(\eta)$ defined in Eq. (58). We now examine solutions to Eq. (62) for the two cases identified earlier: $M^2 < 1$ and $-1 < \eta^+ < 0$; and $M^2 > 1$ and $\eta^+ > 0$.

1. Nonlinear traveling-wave solutions ($M^2 < 1$ and $-1 < \eta^+ < 0$)

Figure 1 shows a schematic plot of $V(\eta)$ versus η for the case where $M^2 < 1$ and $-1 < \eta^+ < 0$. For the purposes of illustration, the values of the specific parameters in Fig. 1 have been chosen to be $M^2 = 0.09$ and $\epsilon_T = 4/15$ in plotting $V(\eta)$ versus η. The corresponding values of η^+, η_m and $V(\eta_m)$ are $\eta^+ = -0.882$, $\eta_m = -0.715$, and $V(\eta_m) = 0.126$. For different choices of values for ϵ_T and $M^2 < 1$, the shape of the $V(\eta)$ versus η curve is qualitatively similar to that shown in Fig. 1. Referring to Fig. 1, when the effective energy E (the red horizontal line in Fig. 1 lies in the interval $0 < E < V(\eta_m)$, Eq. (66) supports nonlinear periodic solutions for $\eta(Z')$ that oscillate as a function of Z'. Here $V(\eta_m)$ is the local maximum of $V(\eta)$, which occurs at $\eta = \eta_m$ in Fig. 1. Depending on system parameters, these nonlinear traveling-wave

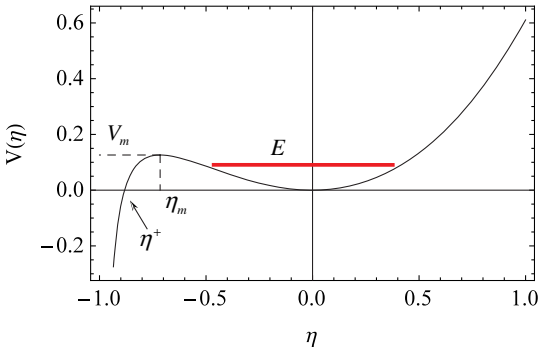

FIG. 1. Illustrative plot of $V(\eta)$ versus η obtained from Eq. (56) for $M^2 = 0.09$ and $\epsilon_T = 4/15$. Here, $\eta^+ = -0.882$, $\eta_m = -0.715$ and $V(\eta_m) = 0.126$.

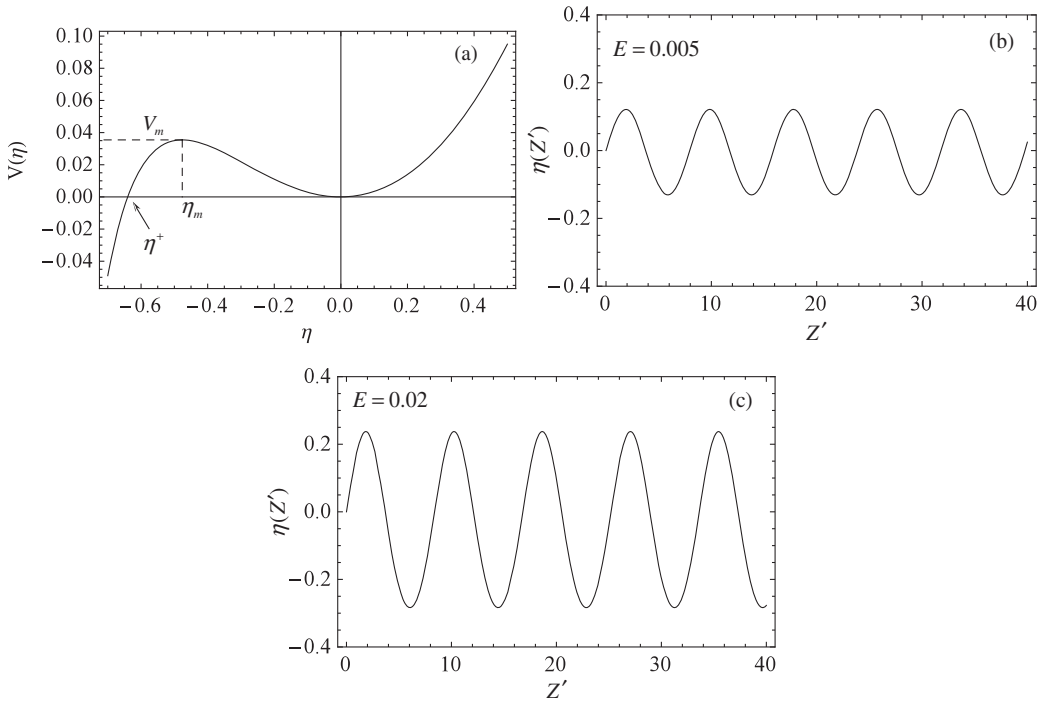

FIG. 2. For $M^2 = 0.36$, $\epsilon_T = 0$, $\eta^+ = -0.64$, $\eta_m = -0.476$ and $V(\eta_m) = 0.0355$, plots are shown for (a) $V(\eta)$ versus η; (b) $\eta(Z')$ versus Z' for $\eta'(0) = 0.1$ and $E = (1/2)[\eta'(0)]^2 = 0.005$; and (c) $\eta(Z')$ versus Z' for $\eta'(0) = 0.2$ and $E = (1/2)[\eta'(0)]^2 = 0.02$.

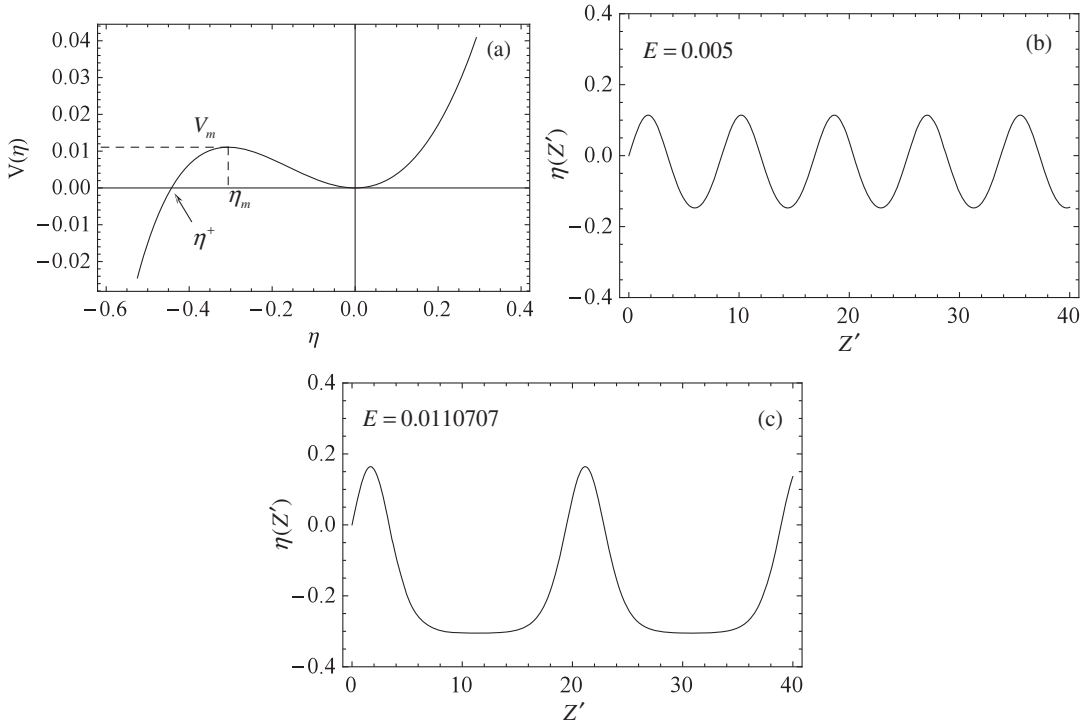

FIG. 3. For $M^2 = 0.36$, $\epsilon_T = 0.8$, $\eta^+ = -0.442$, $\eta_m = -0.306$ and $V(\eta_m) = 0.0111$, plots are shown for (a) $V(\eta)$ versus η; (b) $\eta(Z')$ versus Z' for $\eta'(0) = 0.1$ and $E = (1/2)[\eta'(0)]^2 = 0.005$; and (c) $\eta(Z')$ versus Z' for $\eta'(0) = 0.1488$ and $E = (1/2)[\eta'(0)]^2 = 0.0110707$.

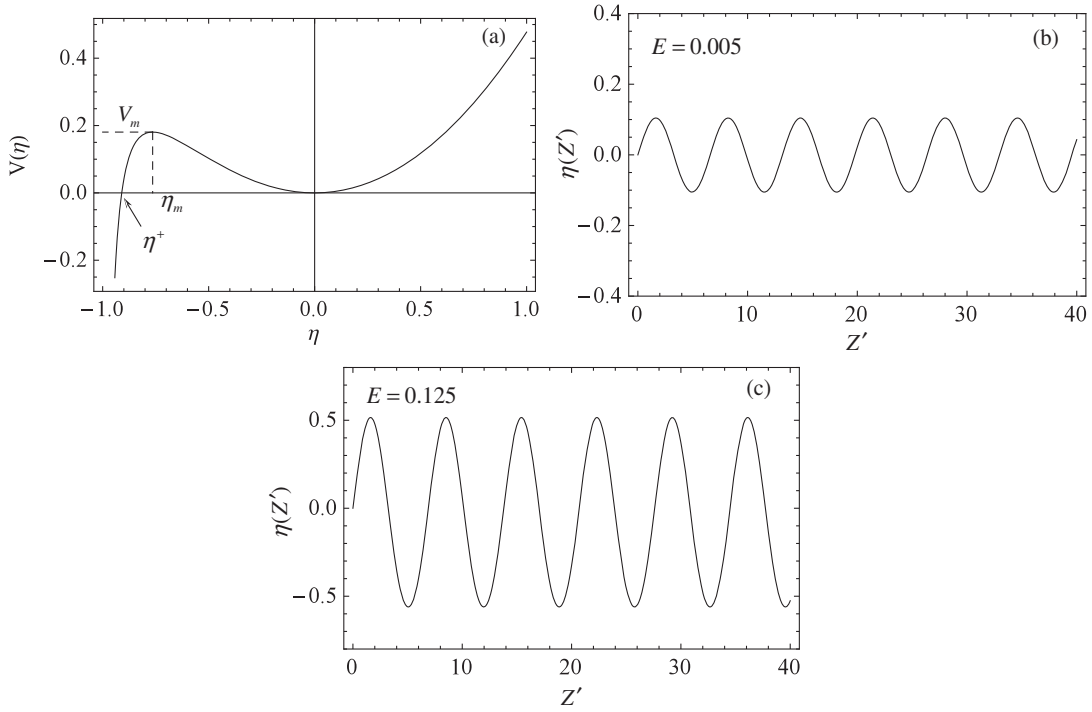

FIG. 4. For $M^2 = 0.09$, $\epsilon_T = 0$, $\eta^+ = -0.91$, $\eta_m = -0.764$ and $V(\eta_m) = 0.181$, plots are shown for (a) $V(\eta)$ versus η; (b) $\eta(Z')$ versus Z' for $\eta'(0) = 0.1$ and $E = (1/2)[\eta'(0)]^2 = 0.005$; and (c) $\eta(Z')$ versus Z' for $\eta'(0) = 0.5$ and $E = (1/2)[\eta'(0)]^2 = 0.125$.

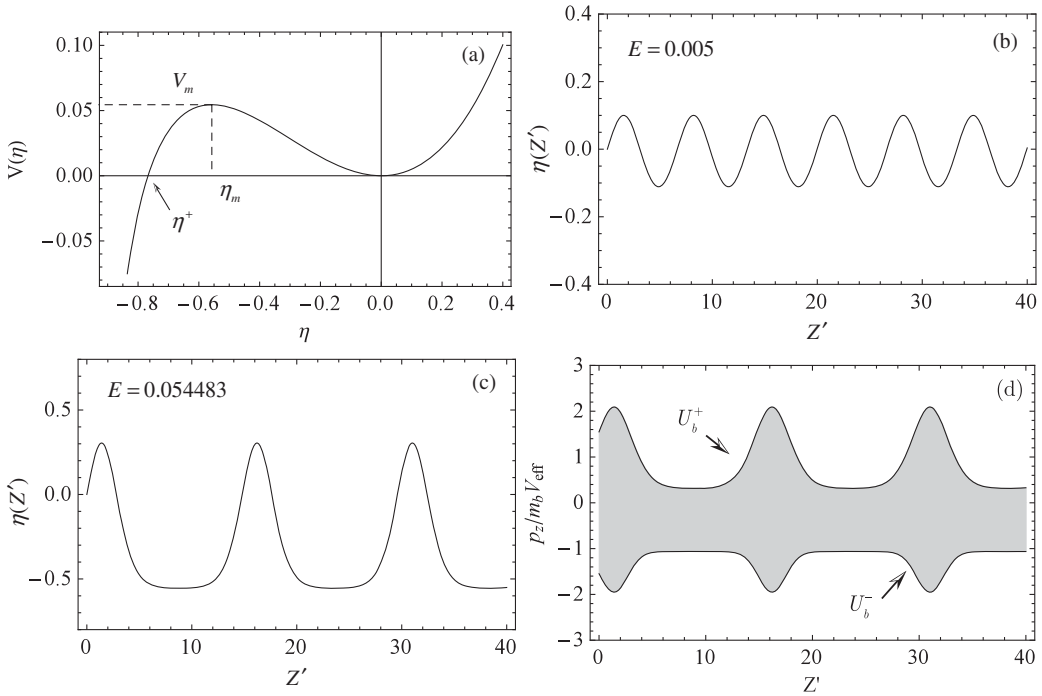

FIG. 5. For $M^2 = 0.09$, $\epsilon_T = 0.8$, $\eta^+ = -0.767$, $\eta_m = -0.557$ and $V(\eta_m) = 0.0545$, plots are shown for (a) $V(\eta)$ versus η; (b) $\eta(Z')$ versus Z' for $\eta'(0) = 0.1$ and $E = (1/2)[\eta'(0)]^2 = 0.005$; and (c) $\eta(Z')$ versus Z' for $\eta'(0) = 0.3301$ and $E = (1/2)[\eta'(0)]^2 = 0.054483$. Shown in (d) is a self-consistent phase-space plot for the waterbag distribution [Eq. (31)] for the choice of system parameters in Fig. 5(c).

solutions can have large amplitude, representing a significant modulation in beam line density.

Referring to the discussion preceding Eq. (58), the boundary conditions used to derive Eqs. (55) and (56) from Eqs. (50) and (51) correspond to

$$\eta(0) = 0 = \eta''(0) \tag{63}$$

for the class of nonlinear periodic wave solutions obtained from Eq. (62) when $M^2 < 1$ and $-1 < \eta^+ < 0$. Furthermore, from Fig. 1 and Eq. (62), we note that $V(\eta = 0) = 0$ and the effective energy E can be expressed as

$$E = \frac{1}{2}[\eta'(0)]^2. \tag{64}$$

Typical numerical solutions for $\eta(Z')$, obtained by integrating Eq. (62) with $V(\eta)$ specified by Eq. (58), are illustrated in Figs. 2–5 for several values of $M^2 < 1$ and ϵ_T, and different values of effective energy level E. These correspond to: $M^2 = 0.36$, $\epsilon_T = 0$, $E = 0.005$, and $E = 0.0110707$ (Fig. 2); $M^2 = 0.36$, $\epsilon_T = 4/15$, $E = 0.005$, and $E = 0.020$ (Fig. 3); $M^2 = 0.09$, $\epsilon_T = 0$, $E = 0.005$, and $E = 0.054483$ (Fig. 4); $M^2 = 0.09$, $\epsilon_T = 4/15$, $E = 0.005$, and $E = 0.125$ (Fig. 5). Close examination of Figs. 2–5 shows several interesting trends. First, for smaller values of M^2, the potential wells are deeper and broader (compare Figs. 2a and 4a, and Figs. 3a and 5a); and for smaller values of ϵ_T, the potential wells are deeper (compare Figs. 2a and 3a, and Figs. 4a and 5a). Furthermore, the nonlinear wave amplitude tends to be larger for smaller values of M^2 (compare Figs. 2a and 3a, and Figs. 4a and 5a), whereas the wavelength dependence on M^2 and ϵ_T tends to be relatively weak (compare Figs. 2, 3, 4, 5). In any case, for $M^2 < 1$, it is clear from Figs. 1–5 that Eqs. (62) and (58) support a broad class of nonlinear traveling-wave solutions for the theoretical model developed here, based on the 1D kinetic waterbag model for intense beam propagation. Indeed, the modulation of the beam line density is about ±50% for the system parameters in Figs. 4(c) and 5(c).

2. *Nonlinear traveling-pulse (soliton) solutions ($M^2 > 1$ and $\eta^+ > 0$)*

We now consider Eqs. (62) and Eq. (58) [or equivalently, Eq. (56)] in circumstances where $M^2 > 1$ and $\eta^+ > 0$. In this case, the effective potential has the qualitative shape illustrated in Fig. 6, which has been plotted for the choice of parameters $M^2 = 9$ and $\epsilon_T = 1/30$. The physically allowed, localized pulse solutions (soliton solutions) corresponds to the energy level

$$E = 0, \tag{65}$$

which is the red horizontal line in Fig. 6, and boundary conditions

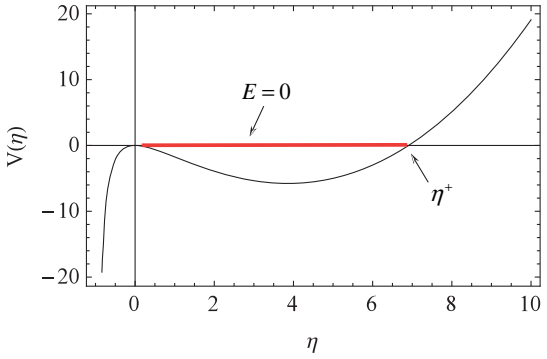

FIG. 6. Illustrative plot of $V(\eta)$ versus η obtained from Eq. (56) for $M^2 = 9$ and $\epsilon_T = 1/50$. Here, $\eta^+ = 6.908$, and the energy level $E = 0$ corresponds to soliton solutions with maximum amplitude $\eta^+ = 6.908$.

$$\eta(Z' = \pm\infty) = 0 = \eta''(Z' = \pm\infty) \tag{66}$$

discussed prior to Eq. (58). Referring to Fig. 6, when Eq. (62) is integrated forward from $Z' = -\infty$ where $\eta = 0$, the perturbed line density, η increases monotonically through positive values to a maximum amplitude η^+ (the soliton amplitude) and then decreases monotonically to $\eta = 0$ when $Z' = +\infty$. The regime where $M^2 > 1$ by a sufficiently large amount corresponds to a strongly nonlinear regime where the density compression is large with $\eta^+ > 1$. On the other hand, when $M^2 - 1 = \epsilon$ is small

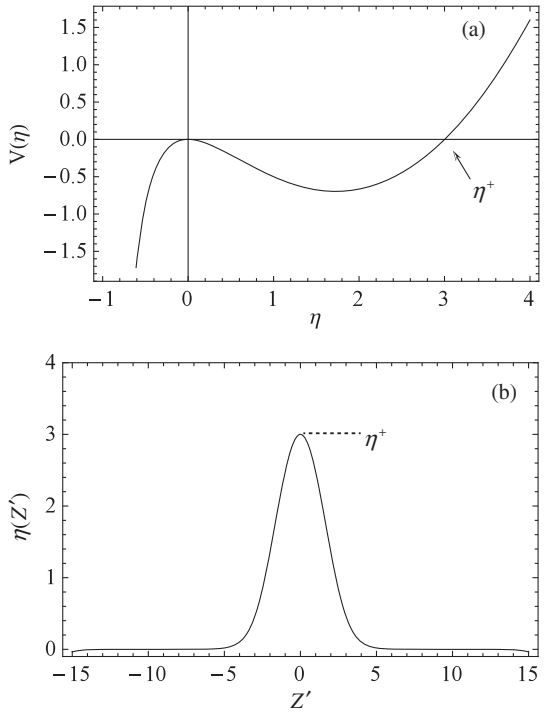

FIG. 7. Plots of (a) $V(\eta)$ versus η; and (b) $\eta(Z')$ versus Z', obtained from Eqs. (56) and (62) for $M^2 = 4$, $\epsilon_T = 0$ and $E = 0$, corresponding to soliton amplitudes $\eta^+ = 3.0$.

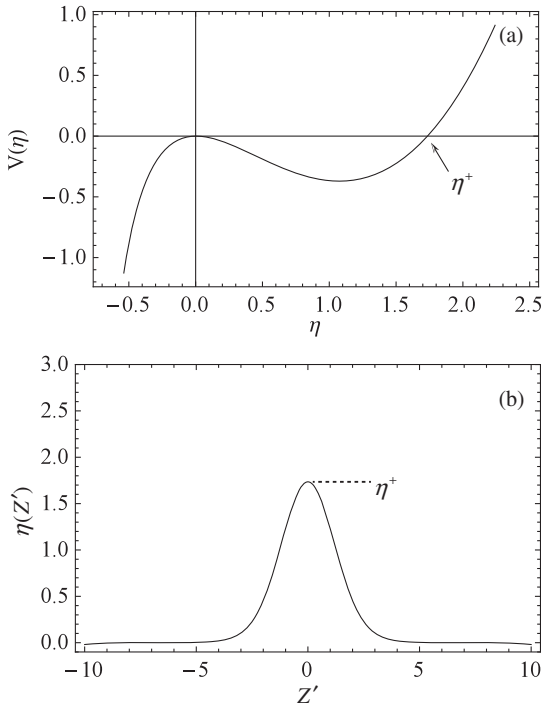

FIG. 8. Plots of (a) $V(\eta)$ versus η; and (b) $\eta(Z')$ versus Z', obtained from Eqs. (56) and (62) for $M^2 = 4$, $\epsilon_T = 4/15$ and $E = 0$, corresponding to soliton amplitudes $\eta^+ = 1.735$.

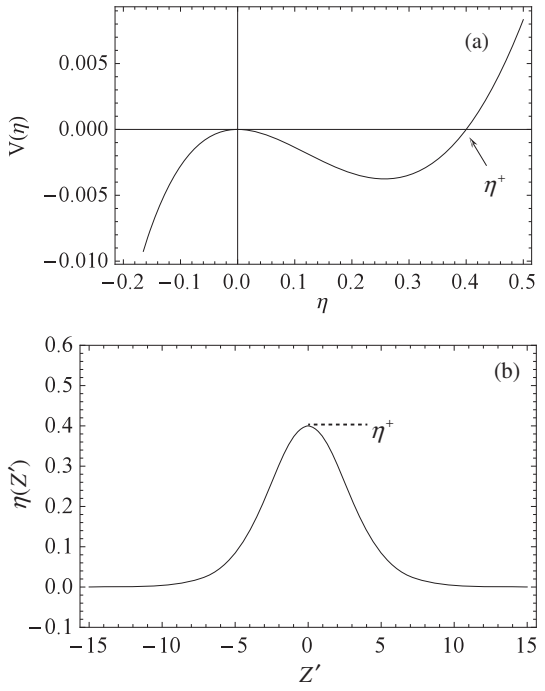

FIG. 9. Plots of (a) $V(\eta)$ versus η; and (b) $\eta(Z')$ versus Z', obtained from Eqs. (56) and (62) for $M^2 = 1.2$, $\epsilon_T = 0$ and $E = 0$, corresponding to soliton amplitudes $\eta^+ = 0.4$.

with $0 < \epsilon \ll 1$, the soliton amplitude is correspondingly small. This will become apparent from the numerical solutions to Eqs. (62) and (58) consistent with Eqs. (65) and (66) presented later in this section in Figs. 7–10.

Typical numerical solutions to Eqs. (62) and (58), subject to Eqs. (65) and (66), are illustrated in Figs. 7–10 for several values of $M^2 > 1$ and ϵ_T. These correspond to: $M^2 = 4$ and $\epsilon_T = 0$ (Fig. 7); $M^2 = 4$ and $\epsilon_T = 4/15$ (Fig. 8); $M^2 = 1.2$ and $\epsilon_T = 0$ (Fig. 9); and $M^2 = 1.2$ and $\epsilon_T = 4/15$ (Fig. 10). Close examination of Figs. 7–10 shows that the soliton amplitude increases with increasing M^2 (compare Figs. 7 and 8 with Figs. 9 and 10), reaching a highly nonlinear regime with $\eta^+ = 3.0$ in Fig. 7 and $\eta^+ = 1.735$ in Fig. 8, where $M^2 = 4$. In contrast, the soliton width trends show a relatively weak dependence on longitudinal velocity spread, as measured by ϵ_T (compare Fig. 8 with Fig. 7, and Fig. 10 with Fig. 9). It is clear from Figs. 7–10 that the soliton solutions to Eqs. (62) and (58) exhibit a strong nonlinear dependence on M^2, and can correspond to highly compressed line density for sufficiently large M^2.

In the special circumstances where M^2 exceeds 1 by a small amount, i.e., $M^2 = 1 + \Delta$ where $0 < \Delta \ll 1$. it is readily shown that Eq. (54) can be approximated for small η by

$$\frac{\partial^2 \eta}{\partial Z'^2} + \left\{ \left[\frac{3}{2} M^2 + \frac{3}{2} \epsilon_T \right] \eta - (M^2 - 1) \right\} \eta = 0. \qquad (67)$$

Equation (67) can be solved exactly for $\eta(Z') = \lambda_b(Z')/\lambda_{b0} - 1$ to give

$$\eta(Z') = \left(\frac{M^2 - 1}{M^2 + \epsilon_T} \right) \mathrm{sech}^2 \left[\frac{1}{2} (M^2 - 1)^{1/2} (Z - MT) \right]. \qquad (68)$$

Note that the soliton amplitude in Eq. (68) is small for $M^2 = 1 + \Delta$ with $\Delta \ll 1$. Also, the $\mathrm{sech}^2\{\cdots\}$ pulse shape in Eq. (68) is similar to the soliton pulse shape obtained from the Korleweg-deVries equation in the weakly nonlinear regime [15].

Finally, it should be noted that the oscillatory solutions obtained from Eqs. (58) and (62) when $M^2 > 1$ and the energy level E in Fig. 6 is negative with $V_{\min} < E < 0$ are not considered here. These solutions are unphysical because they oscillate about a positive nonzero average value of $\bar{\eta} = \bar{\lambda}_b/\lambda_{b0} - 1 > 0$, rather than oscillate about $\bar{\eta} = \bar{\lambda}_b/\lambda_{b0} - 1 \approx 0$, as occurs in Figs. 2–5 when $M^2 < 1$.

In concluding Sec. III, it should be noted that once $\eta(Z')$ is determined from Eq. (62) for specified system parameters, then Eqs. (35), (36), and (52) can readily be used to develop plots of the nonlinearly distorted phase-space boundaries V_b^+ and V_b^-, both for the case of nonlinear traveling wave solutions (Figs. 1–5) and for nonlinear traveling soliton solutions (Figs. 6–10). Normalizing V_b^+, V_b^-, and V_b to the effective sound speed $V_{\mathrm{eff}} = (U_{b0}^2 + U_{bT}^2)^{1/2}$ according to $U_b^+ = V_b^+/V_{\mathrm{eff}}$, $U_b^- = V_b^-/V_{\mathrm{eff}}$, and $U = V_b/V_{\mathrm{eff}}$, Eqs. (35), (36), and (52) give $\eta + 1 =$

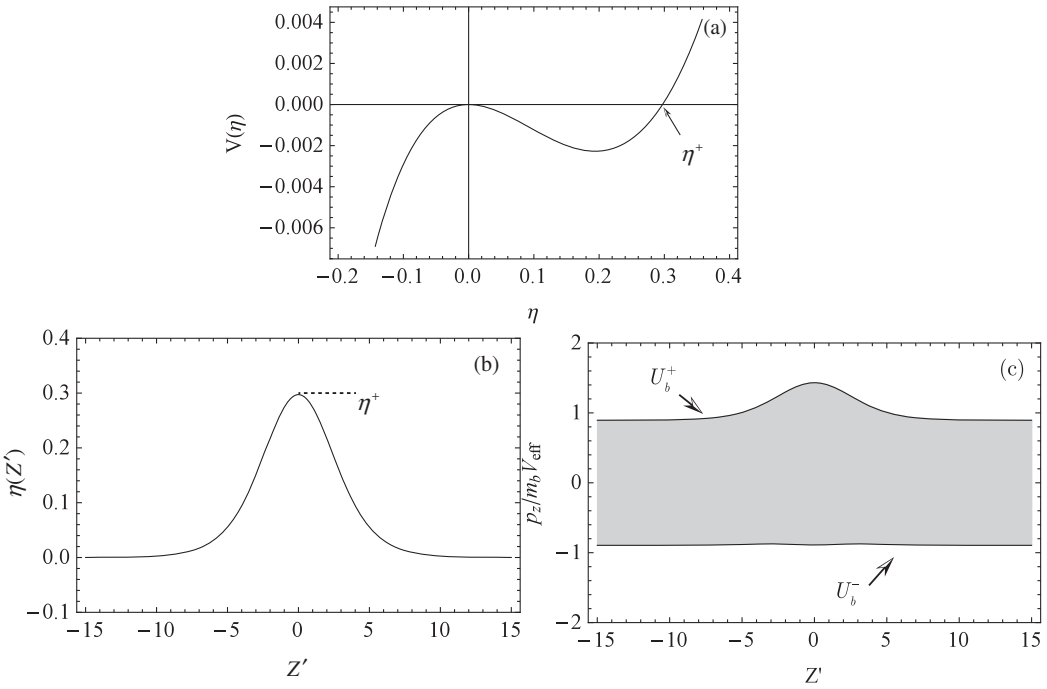

FIG. 10. Plots of (a) $V(\eta)$ versus η; and (b) $\eta(Z')$ versus Z', obtained from Eqs. (56) and (62) for $M^2 = 1.2$, $\epsilon_T = 4/15$ and $E = 0$, corresponding to soliton amplitudes $\eta^+ = 0.297$. Shown in (c) is a self-consistent phase-space plot for the waterbag distribution [Eq. (31)] for the choice of system parameters in Fig. 10(b).

$(Am_bV_{\rm eff}/\lambda_{b0})(U_b^+ - U_b^-)$, and $U = (U_b^+ + U_b^-)/2 = M\eta/(1+\eta)$. For example, for the choice of system parameters and nonlinear traveling-wave solution for $\eta(Z')$ illustrated in Fig. 5(c), shown in Fig. 5(d) is the corresponding self-consistent phase-space plot for the waterbag distribution, which shows clearly how the boundary curves $U_b^+(Z')$ and $U_b^-(Z')$ evolve nonlinearly as the beam line density alternately compresses and decompresses as shown in Fig. 5(c). By contrast, for the choice of system parameters and compressive soliton solution for $\eta(Z')$ illustrated in Fig. 10(b), shown in Fig. 10(c) is the corresponding phase-space plot for the waterbag distribution, which shows how the boundary curves $U_b^+(Z')$ and $U_b^-(Z')$ evolve as the beam line density experiences a single soliton compression with moderately large amplitude.

IV. COHERENT NONLINEAR STRUCTURES OBTAINED FROM FULLY KINETIC G-FACTOR MODEL

The kinetic waterbag model developed in Sec. III of this paper has clearly demonstrated the rich variety of coherent nonlinear structures supported by the 1D kinetic model based on Eqs. (9) and (10) [or equivalently, Eqs. (1) and (2)] for the specific choice of waterbag distribution $F_b(z, p_z, t)$ in Eq. (31). In this section, we examine solutions to Eqs. (9) and (10) for an even broader class of distribution functions $F_b(z, p_z, t)$, recognizing that Eqs. (9) and (10) are Galilean invariant. That is, if we transform variables to a frame of reference moving with constant longitudinal velocity $V_0 = \text{const}$ according to $z' = z - V_0 t$, $p_z' = p_z - m_b V_0$, $t' = t$, then in the new dynamical variables (z', p_z', t'), the equations for $F_b(z', p_z', t')$ and $\langle\phi\rangle(z', t')$ are identical in form to Eqs. (9) and (10). Time-stationary solutions $(\partial/\partial t' = 0)$ in the new variables (z', p_z', t') then correspond to undistorted traveling-wave or traveling-pulse solutions moving with constant velocity $V_0 = \text{const}$ in the original variables (z, p_z, t). The present analysis of Eqs. (9) and (10) parallels the original Bernstein-Greene-Kruskal (BGK) formulation of BGK solutions to the 1D Vlasov-Poisson equations [25,26], except for the fact that Eq. (10), which connects $\langle\phi\rangle(z, t)$ to the line density $\lambda_b(z, t)$, has a very different structure than the 1D Poisson equation.

Referring to Eqs. (9) and (10), we introduce the scaled dimensionless variables (Z, P_z, T) defined by

$$Z = \left(\frac{U_{b0}^2 + U_{bT}^2}{U_{b2}^2}\right)^{\frac{1}{2}} \frac{z}{r_w}, \qquad T = \left(\frac{U_{b0}^2 + U_{bT}^2}{U_{b2}^2}\right) \frac{U_{b2} t}{r_w},$$
$$P_z = \frac{p_z}{m_b (U_{b0}^2 + U_{bT}^2)^{1/2}} = \frac{v_z}{(U_{b0}^2 + U_{bT}^2)^{1/2}} \equiv V_z, \qquad (69)$$

where U_{b0}^2 and U_{b2}^2 are defined in Eq. (3), and $U_{bT}^2 = \text{const}$ is the longitudinal velocity spread characteristic of the distribution function F_b. We further introduce the dimensionless distribution function $\hat{F}_b(Z, P_z, T)$ defined by

$$\hat{F}_b = \lambda_{b0}^{-1} \frac{F_b}{m_b(U_{b0}^2 + U_{bT}^2)^{1/2}}, \tag{70}$$

where $\lambda_{b0} = \text{const}$ is the characteristic line density of the beam particles, e.g., the average value. From Eqs. (69), (70) and the definition of line density $\lambda_b = \int dp_z F_b$, it follows that the perturbation in line density $\eta = \lambda_b/\lambda_{b0} - 1$ can be expressed as

$$\eta(Z,T) = \int dP_z \hat{F}_b(Z,P_z,T) - 1, \tag{71}$$

where the P_z integration covers the range $-\infty < P_z < \infty$ in Eq. (71). Transforming variables according to Eqs. (69) and (70), and making use of Eq. (71), it is readily shown that Eqs. (9) and (10) can be expressed in the new variables as

$$\frac{\partial \hat{F}_b}{\partial T} + V_z \frac{\partial \hat{F}_b}{\partial Z} - \frac{\partial \psi}{\partial Z}\frac{\partial \hat{F}_b}{\partial P_z} = 0, \tag{72}$$

and

$$\psi = \eta + \frac{\partial^2 \eta}{\partial Z^2}, \tag{73}$$

where $\psi(Z,T)$ is the normalized (dimensionless) potential defined by

$$\psi = \frac{e\langle\phi\rangle}{m_b(U_{b0}^2 + U_{bT}^2)^{1/2}}. \tag{74}$$

Equations (72) and (73), where η and $\int dP_z \hat{F}_b$ are related by Eq. (71), constitute coupled nonlinear equations describing the self-consistent evolution of the distribution function $\hat{F}_b(Z,P_z,T)$, normalized potential $\psi(Z,T)$, and normalized perturbed line density $\eta(Z,T)$. Equations (71)–(73) are fully equivalent to the original dynamical equations (9)–(11), and can be used to investigate 1D kinetic properties of the nonlinear beam dynamics over a wide range of system parameters.

Keeping in mind that Eqs. (72) and (73) are Galilean invariant, if we transform Eqs. (72) and (73) from the variables (Z,P_z,T) to a frame moving with normalized velocity $M = \text{const.}$ according to $Z' = Z - MT$, $V_z' = V_z - M$, $T' = T$, then Eqs. (72) and (73) have exactly the same form in the new variables, with (Z,P_z,T) replaced by (Z',P_z',T'), i.e.,

$$\frac{\partial \hat{F}_b}{\partial T'} + V_z' \frac{\partial \hat{F}_b}{\partial Z'} - \frac{\partial \psi}{\partial Z'}\frac{\partial \hat{F}_b}{\partial P_z'} = 0, \tag{75}$$

and

$$\psi = \eta + \frac{\partial^2 \eta}{\partial Z'^2}. \tag{76}$$

Here, $P_z' = V_z'$, and $\hat{F}_b(Z',P_z',T')$ and $\eta(Z',T')$ are related by

$$\eta(Z',T') = \int dP_z' \hat{F}_b(Z',P_z',T') - 1. \tag{77}$$

Therefore, the traveling-pulse or traveling-wave solutions that have a time-stationary profile shape in the primed variables (Z',P_z',T') are determined by setting $\partial/\partial T' = 0$ in Eqs. (75)–(77).

Setting $\partial \hat{F}_b/\partial T' = 0$ in Eq. (75) gives for $\hat{F}_b(Z',P_z')$

$$V_z' \frac{\partial \hat{F}_b}{\partial Z'} - \frac{\partial \psi}{\partial Z'}\frac{\partial \hat{F}_b}{\partial P_z'} = 0, \tag{78}$$

where $\psi(Z')$ and $\eta(Z')$ solve Eq. (76), and $\eta(Z')$ is related to $\hat{F}_b(Z',P_z')$ by Eq. (77). We introduce the energy variable W' defined by

$$W' = \frac{1}{2}V_z'^2 + \psi(Z'). \tag{79}$$

Then the solution to Eq. (78) for $\hat{F}_b(Z',P_z')$ can be expressed exactly as

$$\hat{F}_b(Z',V_z') = \hat{F}_b^{>}(W')\Theta(V_z') + \hat{F}_b^{<}(W')\Theta(-V_z'), \tag{80}$$

where $P_z' = V_z'$, and

$$\Theta(V_z') = \begin{cases} 1, & \text{for } V_z' > 0, \\ 0, & \text{for } V_z' < 0. \end{cases} \tag{81}$$

Note from Eq. (79) that

$$dV_z' = \pm dW'/[2(W'-\psi)]^{1/2}, \tag{82}$$

where $+$ corresponds to $V_z' > 0$, and $-$ corresponds to $V_z' < 0$. Substituting Eqs. (80) and (82) into Eq. (77) gives

$$\eta = \int_\psi^\infty dW' \frac{[\hat{F}_b^{>}(W') + \hat{F}_b^{<}(W')]}{[2(W'-\psi)]^{1/2}} - 1, \tag{83}$$

which relate the perturbation in beam line density $\eta(Z')$ to the potential $\psi(Z')$ and the distribution functions $\hat{F}_b^{>}(W')$ and $\hat{F}_b^{<}(W')$.

To summarize, solutions to the nonlinear Vlasov equation (75) that are time-stationary ($\partial/\partial T' = 0$) in a frame of reference moving with normalized velocity $M = \text{const}$ are determined from (78), which in turn has exact solutions for the distribution function $\hat{F}_b(Z',V_z')$ of the general form given in Eq. (80), where W' is the total particle energy

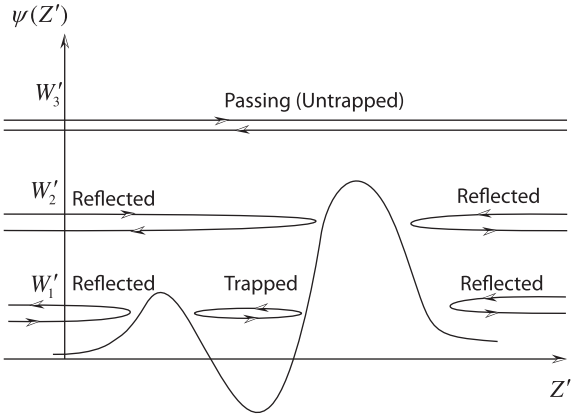

FIG. 11. Illustrative plot of the effective potential $\psi(Z')$ versus Z' occurring in Eq. (33) showing the three classes of particle orbits corresponding to: passing (untrapped) particles with energy W_3'; reflected particles with energy W_2'; and reflected or trapped particles (depending on the range of Z') with energy W_1'. The form of $\psi(Z')$ in Fig. 11 corresponds to an isolated pulse with $\psi(Z' \to \pm\infty) = 0$.

(kinetic plus potential) defined in Eq. (79). Although the class of distributions described by Eqs. (79) and (80) is broad, it should be kept in mind that not all choices of distribution function $\hat{F}_b(W')$ are likely to be physically realized.

To reiterate the main features of the present model, for time-stationary solutions ($\partial/\partial T' = 0$) in the moving frame, the normalized self-field potential $\psi(Z')$ and perturbed line density $\eta(Z') = [\lambda_b(Z') - \lambda_{b0}]/\lambda_{b0}$ are related by Eq. (76), and in turn $\eta(Z')$ is related self-consistently to the distribution function $\hat{F}_b(W') = \hat{F}_b^{>}(W') + \hat{F}_b^{<}(W')$ by Eq. (83), where $W' = (1/2)V_z'^2 + \psi(Z')$ is the particle energy (kinetic plus potential). Therefore, for particles distributed in energy W' according to a specified functional

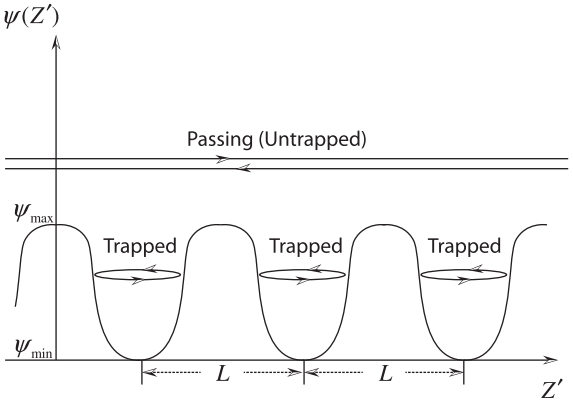

FIG. 12. Illustrative plot of the effective potential $\psi(Z')$ versus Z' for the case where $\psi(Z')$ has a nonlinear periodic waveform with $\psi(Z' + L) = \psi(Z')$, where L is the periodicity length. In the figure, passing particles with energy $W' > \psi_{\max}$ are untrapped, whereas particles with energy $\psi_{\min} < W' < \psi_{\max}$ are trapped and exhibit periodic motion in the potential $\psi(Z')$.

form for $\hat{F}_b(W')$, one can envision calculating self-consistently $\eta[\psi(Z')]$ from Eq. (83), and $\psi(Z')$ from Eq. (76). Once $\psi(Z')$ is determined self-consistently for particles distributed in energy W' according to $\hat{F}_b(W')$, it is both reasonable and informative to examine the motion of an individual "test" particle with energy W' in the self-field potential $\psi(Z')$. For time-stationary potential $\psi(Z')$, particles move on constant energy surfaces with energy $W' = (1/2)V_z'^2 + \psi(Z') = \text{const}$ [see Eq. (79)]. For $W' > \psi(Z')$, the orbit $Z'(T')$ of a particle with energy W' is determined from $dZ'/dT' = V_z' = \pm[2(W - \psi(Z')]^{1/2}$. Keeping in mind that $\hat{F}_b(W')$ is the distribution of particles (in energy) that self-consistently generates the potential $\psi(Z')$, the preceding discussion forms the basis for examining qualitative features of the single-particle motion for different values of W', both for isolated pulse disturbances (Fig. 11), and nonlinear traveling wave distributions (Fig. 12).

Figure 11 shows an illustrative plot of the potential $\psi(Z')$ as a function of Z'. Depending on the values of the energy W' and the range of Z', there are three classes of particle orbits: (i) particles that are reflected from the potential; (ii) particles that are trapped and undergo periodic motion; and (iii) passing (untrapped) particles that do not change direction, but pass over the potential maximum, first slowing down and then speeding up during the motion. For the trapped particles and the reflected particles, it follows that $\hat{F}^{>}(W') = \hat{F}^{<}(W')$ so that

$$\hat{F}_{\rm Tr}(W') = \hat{F}_{\rm Tr}^{<}(W') + \hat{F}_{\rm Tr}^{>}(W') = 2\hat{F}_{\rm Tr}^{<}(W') = 2\hat{F}_{\rm Tr}^{>}(W') \tag{84}$$

and

$$\hat{F}_{\rm Ref}(W') = \hat{F}_{\rm Ref}^{<}(W') + \hat{F}_{\rm Ref}^{>}(W') = 2\hat{F}_{\rm Ref}^{<}(W') = 2\hat{F}_{\rm Ref}^{>}(W'). \tag{85}$$

On the other hand, for the passing (untrapped) particles, $\hat{F}_{\rm Un}^{>}(W')$ and $\hat{F}_{\rm Un}^{<}(W')$ can be specified independently, depending on whether the particles have $V_z' > 0$ or $V_z' < 0$, respectively.

The form of $\psi(Z')$ shown in Fig. 11 corresponds to a stationary isolated pulse in primed variables, with $\psi(Z' = \pm\infty) = 0$. By contrast, Fig. 12 shows a plot of $\psi(Z')$ versus Z' for the case where $\psi(Z')$ has a periodic nonlinear wave structure with

$$\psi(Z' + L) = \psi(Z'). \tag{86}$$

From Fig. 12, trapped particles with energy W' in the range

$$\psi_{\min} < W' < \psi_{\max} \tag{87}$$

exhibit periodic motion. On the other hand, passing particles with energy W' in the range (see Fig. 12)

$$W' > \psi_{\max} \tag{88}$$

correspond to untrapped particles that pass over the potential $\psi(Z')$, periodically speeding up and slowing down, but not changing their direction of motion. Furthermore, for the nonlinear periodic waveform for the potential $\psi(Z'+L)=\psi(Z')$ shown in Fig. 12, it follows from Eqs. (76) and (83) that the waveform for the perturbation in line charge also satisfies $\eta(Z'+L)=\eta(Z')$. Here, $\eta(Z')$ is related to $\psi(Z')$ and the trapped-particle and untrapped-particle distribution functions by Eq. (83), which gives

$$1+\eta = \int_{\psi}^{\psi_{\max}} dW' \frac{\hat{F}_{\rm Tr}(W')}{[2(W'-\psi)]^{1/2}} + \int_{\psi}^{\infty} dW' \frac{\hat{F}_{Un}(W')}{[2(W'-\psi)]^{1/2}}. \tag{89}$$

In Eq. (89), the integration over the trapped-particle distribution $\hat{F}_{\rm Tr}(W')$ is over the interval of W' corresponding to $\psi_{\min} < \psi < W' < \psi_{\max}$, and the integration over the untrapped particle distribution $\hat{F}_{Un}(W')$ is over the interval of W' corresponding to $\psi_{\max} < \psi < W' < \infty$.

Equations (76) and (89) can be used to determine detailed properties of self-consistent nonlinear periodic solutions for $\eta(Z')$ and $\psi(Z')$ for a broad range of choices of $\hat{F}_{\rm Tr}(W')$ and $\hat{F}_{\rm Un}(W')$. Furthermore, depending on system parameters, the amplitudes of the wave perturbations can range from small to moderately large amplitude. For purposes of illustration, the procedure for solving Eqs. (76) and (89) for the case of nonlinear periodic solutions for $\eta(Z')$ and $\psi(Z')$, we consider the special case where $\hat{F}_{\rm Tr}(W')=0$, and the untrapped distribution function has the monoenergetic form

$$\hat{F}_{\rm Un}(W') = A\sqrt{2W'_U}\,\delta(W'-W'_U), \tag{90}$$

where $W'_U = {\rm const}$, $A = {\rm const}$, and $W'_U > \psi_{\max}$ (see Fig. 12). Substituting $\hat{F}_{\rm Tr}(W')=0$ and Eq. (90) into Eq. (89) readily gives

$$1+\eta(Z') = \frac{A}{[1-\psi(Z')/W'_U]^{1/2}}. \tag{91}$$

For present purpose, we choose the normalization constant A in Eq. (91) such that the line density perturbation $\eta(Z') = \lambda_b(Z')/\lambda_{b0} - 1$ and potential perturbation $\psi(Z')$ are simultaneously zero for all Z', i.e., $\eta(Z')=0$ for all Z', when $\psi(Z')=0$. From Eq. (91), this readily gives $A=1$ for the value of the constant A. Squaring Eq. (91) and solving for $\psi(Z')$ when $A=1$ readily gives

$$\psi = W'_U\left[1-\frac{1}{(1+\eta)^2}\right]. \tag{92}$$

Note that Eq. (92) determines $\psi(Z')$ as a function of $\eta(Z')$, which can be substituted into Eq. (76) to solve for $\eta(Z')$.

Similar to the analysis in Sec. III B for the class of nonlinear periodic traveling-wave solutions with $\eta(Z'+L)=\eta(Z')$ and $\psi(Z'+L)=\psi(Z')$, we examine Eqs. (76) and (92) for the case where the boundary conditions correspond to $\eta(Z'=0)=0$ and $[\partial^2\eta/\partial Z'^2]_{Z'=0}=0$. Substituting Eq. (92) into Eq. (76) we readily obtain

$$\frac{\partial^2\eta}{\partial Z'^2} + \eta = W'_U\left[1-\frac{1}{(1+\eta)^2}\right], \tag{93}$$

which can also be expressed as

$$\frac{\partial^2\eta}{\partial Z'^2} + \frac{\partial V}{\partial \eta} = 0, \tag{94}$$

where

$$\frac{\partial V}{\partial\eta} = \eta - W'_U\left[1-\frac{1}{(1+\eta)^2}\right] = \frac{\eta}{(1+\eta)^2}[\eta^2 + (2-W'_U)\eta + (1-2W'_U)]. \tag{95}$$

Note that Eq. (94) has the form of a dynamical equation of motion, with η playing the role of displacement, Z' playing the role of time, and $V(\eta)$ playing the role of an effective potential, or so-called pseudopotential. Making use of Eq. (95), it is readily shown that

$$\frac{\partial^2 V}{\partial\eta^2} = 1 - \frac{2W'_U}{(1+\eta)^3}, \tag{96}$$

and

$$V(\eta) = \frac{1}{2}\eta^2 - W'_U\left[\eta + \frac{1}{1+\eta} - 1\right] = \frac{1}{2}\frac{\eta^2}{(1+\eta)^2}\{\eta + [1-2W'_U]\}, \tag{97}$$

where the constant of integration in Eq. (97) has been chosen so that $V(\eta=0)=0$.

Close examination of Eqs. (93)–(96) shows that Eq. (94) supports oscillatory solutions for $\eta(Z')$ about $\eta=0$ provided $[\partial^2 V/\partial\eta^2]_{\eta=0} > 0$, or equivalently,

$$2W'_U < 1. \tag{98}$$

When the inequality in Eq. (98) is satisfied, the plot of $V(\eta)$ versus η has the characteristic shape illustrated in Fig. 13 for the choice of parameter $2W'_U < 1$. Here, $V(\eta)$ has a minimum at $\eta=0$, and passes through zero at

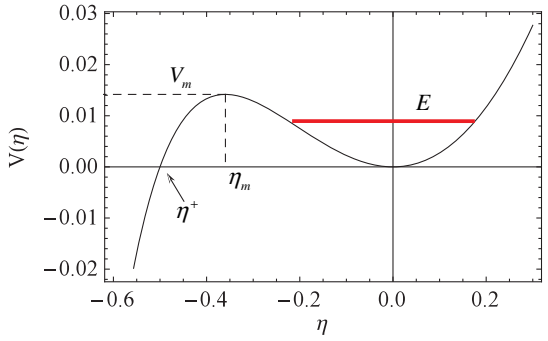

FIG. 13. Plot of $V(\eta)$ versus η obtained from Eq. (97) for $2W'_u = 0.5$ and $\eta^+ = -0.5$. Here, $\eta_m = -0.36$, and $V(\eta_m) = 0.014$. Nonlinear periodic solutions for $\eta(Z')$ exist for energy level E in the range $0 < E < V(\eta_m)$.

$$\eta = \eta^+ = -[1 - 2W'_U], \tag{99}$$

where $V(\eta = \eta^+) = 0$ [see Eqs. (97) and (99)]. Similar to the analysis in Sec. III B, Eq. (94) can be integrated to give the effective energy conservation relation $(1/2)[\partial\eta/\partial Z']^2 + V(\eta) = E = \text{const}$ [see also Eq. (62)], where $E = (1/2)[\eta'(0)]^2$ is the effective energy level. Referring to Fig. 13, Eqs. (94) and (97) support nonlinear periodic oscillatory solutions for $\eta(Z')$ for E in the range $0 < E < V_m$, where $V_m \equiv V(\eta = \eta_m)$ is the local maximum of $V(\eta)$ at $\eta = \eta_m$. For the choice of dimensionless parameter $2W'_u = 1/2$ in Fig. 13, it is readily shown that $\eta_m = -0.360$ and $V_m = V(\eta = \eta_m) = 0.014$.

Recall that the primed variables (Z', V'_z, T') are related to (Z, V_z, T) by $Z' = Z - MT$, $V'_z = V_z - M$, and $T' = T$, where $M = \text{const}$ is the dimensionless velocity of the traveling wave relative to the unprimed frame. Therefore, for a nonlinear wave that is time stationary $(\partial/\partial T' = 0)$ in the primed variables, it is reasonable to identify $W_U{}'$ with $W'_U = (1/2)M^2$ for a monoenergetic beam. In this case, we make the identification $2W'_U < 1$, so the condition for Eqs. (94) and (95) to have nonlinear periodic solutions for $\eta(Z')$ [see Eq. (98)] can be expressed as

$$M^2 < 1. \tag{100}$$

Typical numerical solutions for $\eta(Z')$, obtained by integrating Eq. (94) with $V(\eta)$ specified in Eq. (97), are illustrated in Figs. 14-17 for several choices of $M^2 < 1$ and different values of effective energy level E. These correspond to: $M^2 = 0.5$, $E = 0.005$, $\eta_m = -0.360$, and $V(\eta_m) = 0.014$ (Fig. 14); $M^2 = 0.5$, $E = 0.054883$, $\eta_m = -0.360$, and $V(\eta_m) = 0.014$ (Fig. 15); $M^2 = 0.09$, $E = 0.05$, $\eta_m = -0.764$, and $V(\eta_m) = 0.181$ (Fig. 16); and $M^2 = 0.09$, $E = 0.18$, $\eta_m = -0.764$, and $V(\eta_m) = 0.181$ (Fig. 17). Figures 14–17 illustrate several interesting trends in the nonlinear periodic wave solutions for $\eta(Z')$. [These should be compared with the nonlinear periodic wave

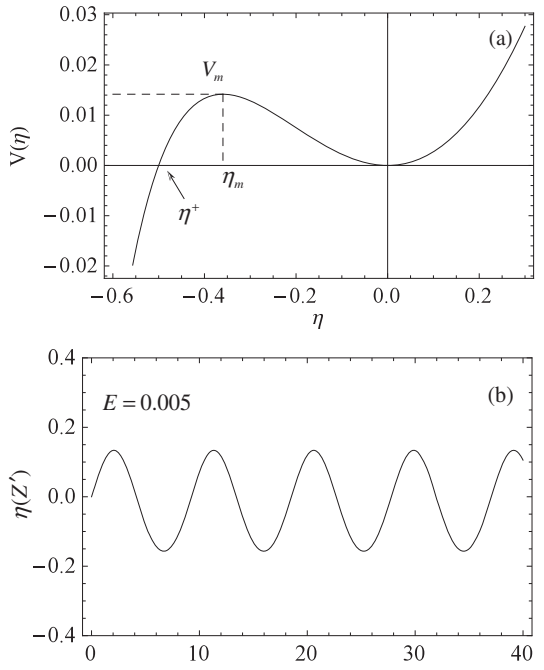

FIG. 14. Plots are shown for (a) $V(\eta)$ versus η, and (b) $\eta(Z')$ versus Z', obtained from Eq. (94) for $M^2 = 0.5$, $\eta'(0) = 0.1$, $E = (1/2)[\eta'(0)]^2 = 0.005$, $\eta^+ = -0.5$, $\eta_m = -0.36$ and $V(\eta_m) = 0.014$.

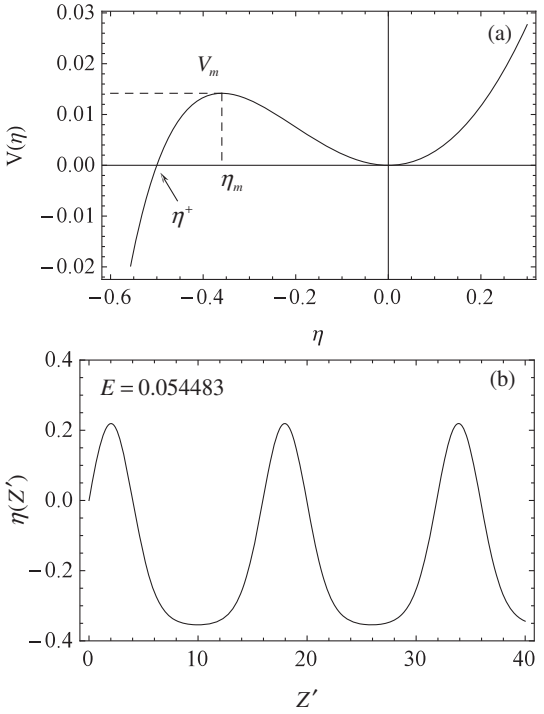

FIG. 15. Plots are shown for (a) $V(\eta)$ versus η, and (b) $\eta(Z')$ versus Z', obtained from Eq. (94) for $M^2 = 0.5$, $\eta'(0) = 0.1863$, $E = (1/2)[\eta'(0)]^2 = 0.054883$, $\eta^+ = -0.5$, $\eta_m = -0.36$ and $V(\eta_m) = 0.014$.

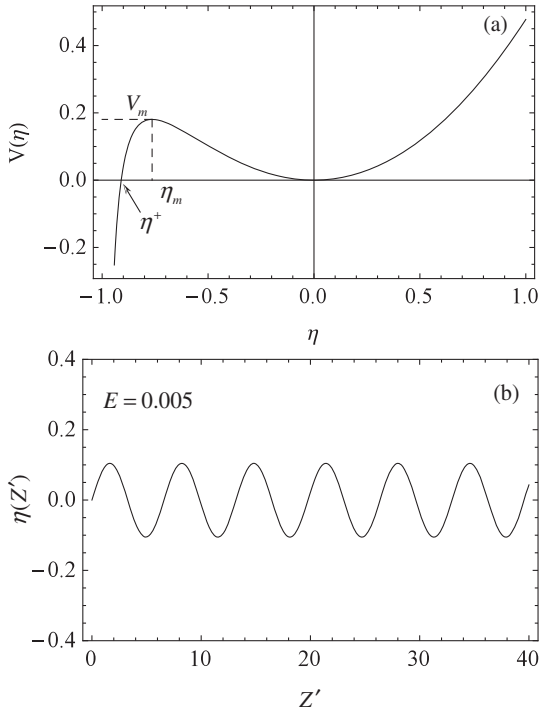

FIG. 16. Plots are shown for (a) $V(\eta)$ versus η, and (b) $\eta(Z')$ versus Z', obtained from Eq. (94) for $M^2 = 0.09$, $\eta'(0) = 0.1$, $E = (1/2)[\eta'(0)]^2 = 0.05$, $\eta^+ = -0.91$, $\eta_m = -0.764$ and $V(\eta_m) = 0.181$.

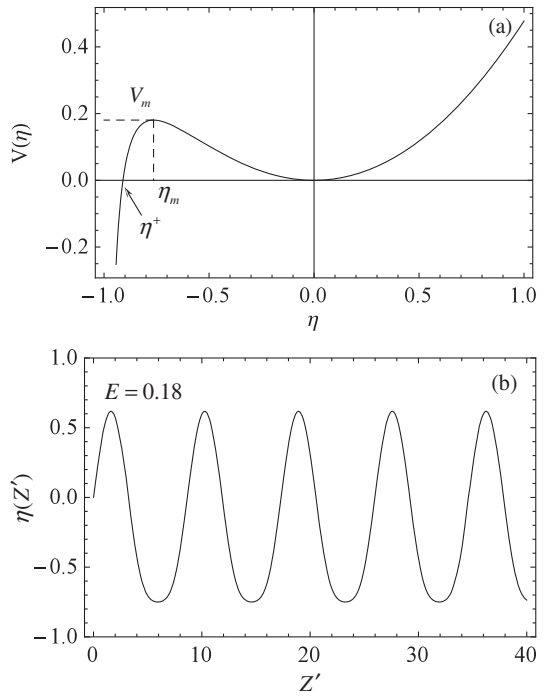

FIG. 17. Plots are shown for (a) $V(\eta)$ versus η, and (b) $\eta(Z')$ versus Z', obtained from Eq. (94) for $M^2 = 0.09$, $\eta'(0) = 0.6$, $E = (1/2)[\eta'(0)]^2 = 0.18$, $\eta^+ = -0.91$, $\eta_m = -0.764$ and $V(\eta_m) = 0.181$.

solutions in Figs. 2–5 obtained in Sec. III for the kinetic waterbag model.] First, for smaller values of M^2, the potential wells are deeper and broader (compare Figs. 14a and 15a with Figs. 16a and 17a). Furthermore, the nonlinear wave amplitudes tend to be large for sufficiently large values of energy level E in the effective potential well (compare Figs. 15 and 17 with Figs. 14 and 16).

V. CONCLUSIONS

In this paper, the 1D kinetic model developed in Ref. [14] was used to describe the nonlinear longitudinal dynamics of intense beam propagation, allowing for moderate-to-large-amplitude modulation in the charge density of the beam particles. Particular emphasis has been placed on investigating detailed properties of nonlinear pulselike (soliton) and periodic traveling-wave disturbances propagating with constant normalized velocity $M =$ const relative to the beam frame. The 1D kinetic formalism [14] was briefly summarized in Sec. II A, and exact (local and nonlocal) nonlinear conservation constraints were derived in Sec. II B for the conserved particle number, momentum, and energy per unit length of the beam, making use of the nonlinear Vlasov equation for $F_b(z, p_z, t)$ in Eq. (1) and the expression for $\langle E_z\rangle(z,t)$ in Eq. (2). Removing the assumption of weak nonlinearity made in Ref. [15], Sec. III made use of the fully nonlinear kinetic waterbag model to investigate detailed properties of traveling nonlinear disturbances propagating with velocity $M =$ const relative to the beam frame. In normalized variables, $Z' = Z - MT$ and $T' = T$, the waveform of the disturbance was assumed to be time-stationary $(\partial/\partial T' = 0)$ in the frame moving with velocity $M =$ const. Nonlinear solutions were examined over a wide range of system parameters for both traveling-pulse (soliton) and nonlinear traveling-wave solutions in which the modulation in beam density was large-amplitude, corresponding to a strongly bunched beam. Finally, in Sec. IV we examined the kinetic model based on Eqs. (9) and (10) [equivalent to Eqs. (1) and (2)] for an even broader class of distribution functions $F_b(z, p_z, t)$. The analysis in Sec. IV parallels the original Bernstein-Greene-Kruskal (BGK) formulation of BGK solutions to the 1D Vlasov-Poisson equations [25,26], except for the fact that Eq. (10), which connects the effective potential $\langle\phi\rangle(z,t)$ to the line density $\lambda_b(z,t)$, has a very different structure than the 1D Poisson's equation used in the original BGK analysis. Depending on the choices of trapped-particle and untrapped-particle distribution functions, the kinetic model described in Sec. IV supports a broad range of nonlinear pulselike (soliton) solutions and periodic traveling-wave solutions that have stationary waveform in a frame of reference moving with velocity $M =$ const relative to the beam frame. Similar to Sec. III, the modulation in beam line density can have large amplitude, corresponding to a strong

bunching of the beam particles. Specific examples were considered in Sec. IV corresponding to nonlinear periodic traveling-wave solutions of Eqs. (9) and (10).

In summary, the analysis in Secs. III and IV has identified a broad class of nonlinear traveling-wave and traveling-pulse (soliton) solutions with time-stationary waveform using a one-dimensional kinetic model based on Eqs. (1) and (2) [14]. Properties of these coherent nonlinear structures depend on the self-consistent interaction of the beam particles with the conducting wall through the geometric factors g_0 and g_2 occurring in Eqs. (2) and (3). Properties of the coherent structures also depend on the detailed distribution of particles in phase space (z, p_z). For example, coherent traveling-wave structures can evolve as the nonlinear saturated state of mild or strong two-stream instability driven by a double-peaked distribution of beam particles in momentum space p_z. The linear (small-signal) theory for collective excitations based on Eqs. (1) and (2) has been developed in Sec. IV of Ref. [14], and will be explored in future studies as a basis for collective excitation of the class of coherent nonlinear structures described in the present article.

ACKNOWLEDGMENTS

This research was supported under the auspices of U.S. Department of Energy Contract No. DE-AC02-09CH11466 with the Princeton Plasma Physics Laboratory.

[1] R. C. Davidson and H. Qin, *Physics of Intense Charged Particle Beams in High Energy Accelerators* (World Scientific, Singapore, 2001).
[2] M. Reiser, *Theory and Design of Charged Particle Beams* (Wiley, New York, 1994).
[3] A. W. Chao, *Physics of Collective Beam Instabilities in High Energy Accelerators* (Wiley, New York, 1993).
[4] D. A. Edwards and M. J. Syphers, *An Introduction to the Physics of High Energy Accelerators, 1993* (Wiley, New York, 1993).
[5] J. D. Lawson, *The Physics of Charged-Particle Beams* (Oxford University Press, New York, 1988).
[6] T. P. Wangler, *Principle of RF Linear Accelerators* (John Wiley & Sons, New York, 1998).
[7] I. Hofmann, *Z. Naturforsch. Teil A* ***37A****, 939 (1982).*
[8] I. Hofmann, Laser Part. Beams **3**, 1 (1985).
[9] R. Fedele, G. Miele, L. Palumbo, and V. Vaccaro, Phys. Lett. A **179**, 407 (1993).
[10] L. K. Spentzouris, J. F. Ostiguy, and P. L. Colestock, Phys. Rev. Lett. **76**, 620 (1996).
[11] O. Boine-Frankenheim, I. Hofmann, and G. Rumolo, Phys. Rev. Lett. **82**, 3256 (1999).
[12] H. Schamel, Phys. Rev. Lett. **79**, 2811 (1997).
[13] H. Schamel and R. Fedele, Phys. Plasmas **7**, 3421 (2000).
[14] R. C. Davidson and E. A. Startsev, Phys. Rev. ST Accel. Beams **7**, 024401 (2004).
[15] R. C. Davidson, Phys. Rev. ST Accel. Beams **7**, 054402 (2004).
[16] R. C. Davidson, H. Qin, S. I. Tzenov, and E. A. Startsev, Phys. Rev. ST Accel. Beams **5**, 084402 (2002).
[17] R. C. Davidson, *Methods in Nonlinear Plasma Theory* (Academic Press, New York, 1972).
[18] K. V. Roberts and H. L. Berk, Phys. Rev. Lett. **19**, 297 (1967).
[19] F. Hohl and M. R. Feix, Astrophys. J. **147**, 1164 (1967).
[20] D. Kordeweg and G. de Vries, Philos. Mag. Ser. 5 **39**, 422 (1895).
[21] H. Washimi and T. Taniuti, Phys. Rev. Lett. **17**, 996 (1966).
[22] C. S. Gardner, J. M. Greene, M. D. Kruskal, and R. M. Miura, Phys. Rev. Lett. **19**, 1095 (1967).
[23] E. Ott and R. Sudan, Phys. Fluids **12**, 2388 (1969).
[24] R. C. Davidson, *Methods in Nonlinear Plasma Theory* (Ref. 17), p. 19.
[25] I. B. Bernstein, J. M. Greene, and M. D. Kruskal, Phys. Rev. **108**, 546 (1957).
[26] R. C. Davidson, *Methods in Nonlinear Plasma Theory* (Ref. 17), p. 72.